Bárbara Patricio Calapez Sabido Falcão
Bachelor in sciences of chemical and biochemicalengineering

Development of a proof of concept of a biosensor based on vesicles adhesion

Dissertation submitted in partial fulfillment
of the requirements for the degree of

Master of Science in
Chemical and Biochemical Engineering

Adviser: Pietro Cicuta, Professor,
University of Cambridge

Co-adviser: Lorenzo Di Michele, Research Fellow, Imperial College London

Examination Committee

Chairperson: Isabel Maria Rôla Coelhoso,
Professora auxiliar do Departamento de Química da FCT UNL

Raporteur: Ana Cecília Afonso Roque,
Prefessora associada do Departamento de Química da FCT UNL

Member: Mário Fernando José Eusébio
Professor auxiliar do Departamento de Química da FCT UNL

FACULDADE DE CIÊNCIAS E TECNOLOGIA
UNIVERSIDADE NOVA DE LISBOA

Setembro, 2019

Bárbara Patrício Calapez Sabido Falcão
Bachelor in sciences of chemical and biochemical engineering

Development of a proof of concept of a biosensor based on vesicles adhesion

Dissertation submitted in partial fulfillment of the requirements for the degree of
Master of Science in
Chemical and Biochemical Engineering

UNIVERSITY OF
CAMBRIDGE

Professor [Pietro Cicuta], Supervisor

Dr [Lorenzo Di Michele], Co-supervisor

Development of a proof of concept of a biosensor based on cell adhesion

This document was created using the (pdf)LaTeX processor, based in the "novathesis" template[1], developed at the Dep. Informática of FCT-NOVA [2].
[1] https://github.com/joaomlourenco/novathesis [2] http://www.di.fct.unl.pt

Dedico esta tese à minha família.

Acknowledgements

I want to thank to FCT where I studied and spend most of my time for the last five years.
I want to thank to my supervisor Pietro Cicuta for accepting me as intern in this group, it was really a privilege to work with all, thank you for your kindness and availability every time I needed. I want to thank also to my co-supervisor Lorenzo D. Michele for the wonderful way he guided me throughout this six months, always in good mood with new solutions and time for me, thank you very much!
Also my supervisor and teacher in Portugal, Mario Eusébio that was a very important person during my degree since we met in projecto I. Always aware of my work and available to answer my calls. Thank you, thank you!
I want to thank to all my labmates and friends that were so patient and welcomed me so well in this group, in special to Roger Rubio whose orientation was incredible and endless patience with all my doubts and training even when the time was tight, your help was crucial for this work!
Alexandra Gabriel I need to thank you for your emotional support during this months here. Our talks were always very good to clean my mind! Also you were the first talking to me, always with that sweet smile and kindness!
I also want to thank my family that provide me all the conditions for me to study and always supported me in special in the last semester so I could do this internship. In special my parents, Bárbara and Rui Falcão for all the love support. I want to thank my boyfriend Tomás because thanks to him I applied to come to Cavendish and I had this wonderful experience, also he was always by my side when I needed in special during this last weeks that I've been working a lot and could not manage time with anything else but my thesis, thanks a lot for all your support!
Now I would also like to thank my friends Mafalda, Inês and Juliana that were a very important support while I was in Cambridge, with our endless calls, and jokes to make me happy when I was sad! Also during my degree they were an incredible support and companions with whom I did all of my works and projects and were the best group I ever worked with! Thank you to all for making this path so much better and easy! For making me a person so proud of my choices! Thank you!

Abstract

Biosensing is an important field of study nowadays because of its application in a wide range of industries such as medical, food industry, environment and agriculture. This leads to a constant need of new technologies to open the applications range or to optimize previous applications. Electrochemical biosensors are portable, sensitive, low costed and require small amounts of sample which make them very interesting for studying and finding new solutions of make it even easier and cheaper. DNA is an impressive molecule that can adopt different configurations, its sequence can be design and is possible to predict its behaviour in specific conditions. This makes it a very appealing tool to develop fields such as biosensing.

DNA can mediate cell adhesion and this is one of the advantages explored throughout this work.

The aim is to engineer a proof-of-concept biosensor via impedance measurements.

In a conductive media the ions move free in solution, but in presence of adhering vesicles the free space decreases and the motion of ions is blocked by the formed structures. This generates a difference in the impedance which is the readable electrical signal.

In this work microfluidic device was designed and optimised to perform impedance measurements of liquid samples, but mostly targeted to sense vesicles adhesion. Moreover, a DNA linking system was successfully designed, characterized, and interfaced with vesicle systems.

Despite having promising results towards a functional biosensor, further work is required to probe appropriate controls that confirm that vesicle adhesion and aggregation are responsible for the changes detected in impedance measurements. Finally, this system can be further interfaced with DNA aptamers towards broadening the range of applications by creating a new method of sensing DNA, proteins, ions, or enzymes.

Keywords: Biosensors, Impedance, Vesicles adhesion, DNA aptamers

Resumo

Os biosensores são uma importante área de estudo nos dias de hoje dadas as suas inúmeras aplicações em indústrias como a indústria médica, alimentar, ambiental e agricula. Isto leva a uma constante necessidade de novas tecnologias, para aumentar as suas aplicações, ou desenvolver outras já existentes.
Os biosensores electroquímicos são portateis, sensiveis, têm baixo custo e precisam de pequenas amostras para funcionar, o que faz destes alvo de estudo para tentar desenvolver novas maneiras, mais faceis e mais baratas de aplicar esta tecnologia.
O ADN é uma molécula extraordinária que consegue adquirir configurações variadas, pode ser desenhado e é possivel prever o seu comportanment em condições especificas. Este pode ser desenhado para mediar adesão entre vesículas e essa é a vantagem explorada neste trabalho.
O objectivo é desenvolver uma prova-de-conceito de um biosensor através de medições de empidência.
Um meio condutor permite que os iões se mouvam livremente em solução, mas na presença de vesículas que se agregam por adesão através de pontes de ADN o espaço livre diminui e o movimento de iões é de certa forma bloqueado. Esta diminuição causa uma diferença na impidência o que é um signal mensurável.
Neste trabalho foi desenhado e optimisado um dispositovo microfluidico usado como plataforma para realizar medições de empidência de amostras liquidas, mas especialmente dirigido a medições de adesão entre vesículas lipídicas.
Foi também desenhado, com sucesso, um sistema de ADN que foi caracterizado e testado com o sistema de vesículas. Apesar de ter apresentado um resultado promissor no sentido de um biosensor funcional, trabalho futuro tem que ser feito para aplicar os controlos apropriados que confirmem que as vesículas aderem e que esta agregação é responsável pelas mudanças detectadas na impidência medida. Por fim este sistema pode futuramente ser interligado com sensores de ADN no sentido de abrir portas a outras applicações criando um novo método de sentir ADN, proteínas, iões ou enzimas.

Palavras-chave: Biosensores, Empidência, Vesículas, Sensores de ADN

Contents

List of Figures

List of Tables

Listings

Acronyms

4-CN	4-chloro-1-naphto.
CV	cyclicvoltametry.
DOPC	1,2-di-(9-octadecenoyl)-sn-glycero-3-phosphocholine.
EIS	eletrochemical impedance spectroscopy.
GUV	Giant Unilamellar Vesicles.
HER-3	human epidermal growth factor receptor-3.
HRP	horseradish peroxidase.
ITO	Indium Tin Oxide.
LUV	Large Unilamellar Vesicles.
MDM2	Murine double minute 2.
PBS	phosphate buffer saline.
PDMS	Polydimethylsiloxane.
PGMEA	Propylene glycol monomethyl ether acetate.
PSA	prostate-specific antigen.
SUV	Smal Unilamellar Vesicles.
tBLMs	Peptide-tethered lipid membranes.

Chapter 1

Motivation and Framework

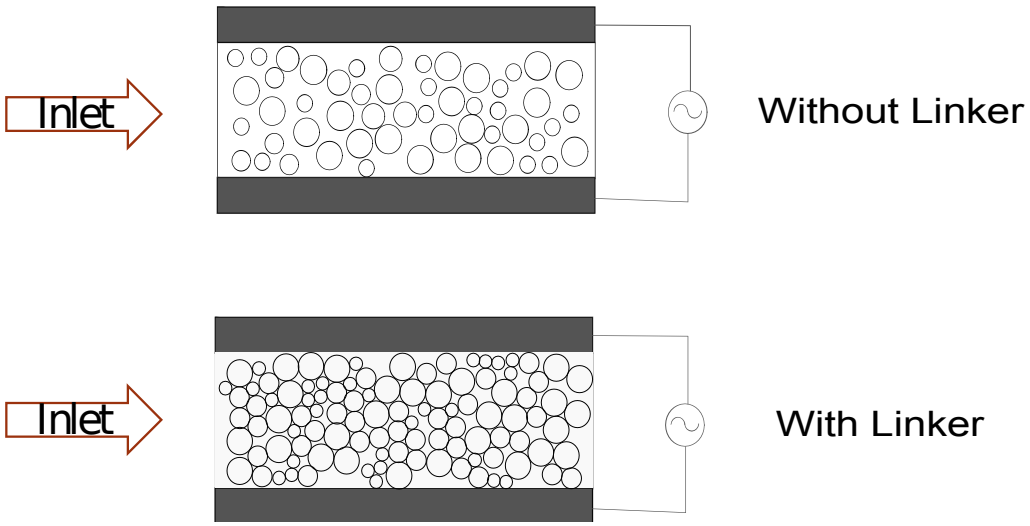

Figure 1.1: Image of a general sensor: One electrode on each side, vesicles suspension between electrodes and AC current applied. This image represents both scenarios, with and without linker.

The concept of biosensing was first approached in the early 1900s by M. Cremer, who demonstrated the proportionality between the concentration of an acid and its electric potential rising amongst the fluids on each side of the membrane [1]. This type of analysis has now increased its range of applications over the years with the embracing of drug discovery, disease detection, environmental monitoring, soil quality investigations, and food and water quality management [1–3].

A biosensor is a device that enables measuring a biological response, such as enzymatic reactions, binding of antibodies, and DNA interactions, by generating signals that are

proportional to the concentration of the molecule of interest, so-called analyte, in the reaction. As discussed previously, one of the analytes that will be probed for is DNA, and this technique can be implemented by anchoring DNA nanostructures to lipid bilayer membranes of vesicles in suspension, which in turn are free to bind to each other in presence of a DNA strand (linker) complementary to each anchored structure. This linker will enable adhesion between vesicles and will be used as analyte. The binding, or adhesion, of vesicles is readily measured with two electrodes with vesicle suspension in between, as shown in Figure 1.1. Vesicles are suspended in a buffer that contains salt and sugar, the salt when in solution dissociates in ions that are free in solution. When an electric field is applied to this solution ions start moving faster and going torwards electrodes depending on its charge. this motion creates a signal. Resistance is the inverse of conductivity that is proportional to salt concentration. In a system with control adhesion, DNA functionalized vesicles move freely in the buffer, because the DNA strands does not stick to each other without a presence of a linker. When a linker is added that triggers the adhesion and the vesicles suspension start creating a vesicle matrix that blocks the ions motion in solution, once the ions can not move as before the resistance signal increases, this system is working as a biosensor that, in this case, is sensing DNA linker. The versatility o DNA is that it can be sensible to a wide vary of molecules. This easy and low-cost system can be a biosensor to other analytes.

Lipid-based vesicles are widely used as model systems in biomedical sciences since they display properties that are similar to those of the cell membrane. Moreover, they can be rendered to undergo binding and aggregation in the presence of specific linking moieties. These are, for instance, interacting systems such as streptavidin-biotin, TCR [4] or collagen [5]. Of particular interest, a linking system can be programmably designed using the tools of DNA Nanotechnology, in which the specific Watson-Crick interactions can be harnessed to promote or disrupt adhesion. Lipid vesicles can be classified in three categories by virtue of their size: Giant Unilamellar Vesicles (GUVs) with dimensions ranging from 1 - 100 μm, Large Unilamellar Vesicles (LUVs) in which the sizes dwell between 100 - 1000 nm, and Small Unilamellar Vesicles (SUVs) falling in the 20 - 100 nm scale. Lipid vesicles are widely used in biomedical sciences due to its similar properties to the cell membrane, they also have aggregation potential either or not in presence of free linkers. There are three ranges of lipid vesicles, giant unilamellar vesicles (GUVs) with sizes ranges 1-100 μm, large unilamellar vesicles (LUVs) with size ranges 100-1000 nm and small unilamellar vesicles (SUVs) with size ranges 20-100 nm.
The functionalization of vesicles with synthetic DNA strands, or tethers, renders them able to adhere with each other and display aggregation capabilities. This process is heavily dependent on well-characterised factors such as temperature, concentration of linkers, or even external stimulus (e.g. electric field). Studies on the impact temperature has within vesicle adhesion have resulted in notions such as the counter-intuitive thermal

response of DNA-mediated aggregation of GUVs. The authors observed that in a low-temperature regime, isolated vesicles become turgid spheres, but upon cooling, the patch between adhered GUVs increases [6].
Considering three characteristic parameters, as in Figure 1.2 of the adhesion between vesicles, such as contact angle (θ), patch area (Ap) and bond distance (D). Their behaviour was assessed upon heating and cooling. The latter showed that both the contact angle and the adhesion patch increased with temperature in an inversely proportional fashion to the bond distance, which decreased with temperature. This occurrence is due to the defformable morphology of vesicles with increasing temperature.

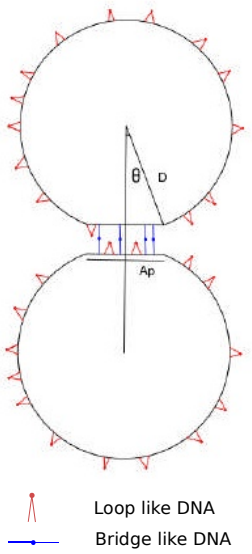

Figure 1.2: Vesicles Adhesion with bridge-like DNA structures. Figure reproduced from [6]

Other work focused on the modulation of vesicle adhesion mediated by electric fields [7]. In this case, the GUVs were prepared via electroformation, as described in section 3.1.1, using two types of lipids: DOPC, with zwitterionic nature, and DOPC, which has a negative contribution to the surface charge. In this system, the GUVs adhere to a planar electrode substrate coated with indium-tin-oxide (ITO). In the absence of a DC electric field, the GUVs diffused freely, and started to adhere at a voltage of 0.8 V. As the external voltage increased, a smooth regulation of the adhesion was observed. Upon removing the potential, the vesicles recovered their ability to freely diffuse and their previous spherical shape.
On the other hand, the morphological and mechanical responses of single GUVs has been studied when adhering to a flat supported lipid bilary (SLB). The authors investigated different concentrations of ligand molecules that were able to mediate the membrane-membrane adhesion [8]. This design included the usage of biotin-functionalized DNA constructs anchored to lipid bilayer membranes via cholesterol molecules. The bridges

between the receptors are formed by biotin-streptavidin interactions, thereby forming multimeric complexes that feature one to four receptors per ligand. With this system, stable adhesion was only observed in a well-defined concentration range of streptavidin. As a consequence, the adhered vesicles display a large increase in membrane tension. Furthermore, it was also possible to identify that the average unbinding rate of ligands is lower at low streptavidin concentrations.

Microfluidics refers to a technology for manufacturing minaturized devices containing micron-sized chambers and tunnels through which fluid is flowed or contained. With the notions above in mind, the approach in [8] can be further studied to create a system where a suspension of GUVs under an electric field is used to probe the presence of a given analyte. This proof-of-concept can be achieved by mediating the adhesion of DNA-functionalized GUVs via DNA ligands, or linkers that freely diffuse in solution. Moreover, this can be measured in a microfluidic device, which structure entails suitable conditions for signal acquisition and very small amounts of sample. The proposal consists in probing the aggregation state of vesicles depending on the linker presence. Through a direct process of vesicle aggregation it is possible to engineer a device where the input is the analyte to be tested and the response is the measured impedance. Within the device, a chamber will contain a suspension of GUVs enclosed by electrodes that will enable the impedance measurements. When the analyte, or linker, is inserted, the binding and adhesion begins thereby creating bridges between vesicles. This results in the suspension of GUVs turning into a matrix network of vesicles, which will in turn limit the diffusion of ions under the electric

The main components of the device are Polydimethylsiloxane (PDMS) and glass coverslips to contain the GUV suspension, electrodes, and the equipment to measure the impedance that is analog discovery 2 osciloscope, logic analyser a power supply from digilent, the software used to work with the equipment was waveform.

All of this materials are low-priced when compared to other commonly used methods such as absorbance spectroscopy, which can determine DNA concentration in samples. This also provides the advantage of circumventing the need for microscopes to readily observe the aggregation of vesicles that can be sensed by the device, besides the main goal of build a biosensor applicable to a wide kind of analytes. This work aims at engineering a device through which, via impedance measurements, the assessment of impedance differences conveys the presence of linker in the suspension. This provides a direct response from a novel biosensor, and the system can be extended to target virtually any analyte for which a suitable DNA linker, or aptamer, is available to interface with the anchoring DNA nanostructures. Aptamers are oligonucleotides molecules that bind to specific target molecules, nucleic acids that are engineered to bind to a specific molecule such as proteins nucleic acids and even cells. These are the species that make sensing with DNA so promising, because of the possibility to design it to all of possible analytes, and will be an important part in this work further development. In this work will be developed

a proof-of-concept of a biosensor based on DNA mediated adhesion of vesicles. The adhseion will be triggered by a DNA linker that starts the aggregation and consequently a structure of vesicles that blocks the way for the ion motion when applied an AC current. This creates a change in the impedance measured in the system. This system will be built in a microfluidic device.

Chapter 2

Introduction

This work will be focused in biosensing with a new approach suggested. This includes DNA nanotechnology with lipid vesicles and impedance measurements. In this chapter is focused on deeply understand each part of the work separately and the connection between them.

2.1 Biosensing

M. Cremer first approach lead to in 1922 registration of the first pH electrode by Walter S. Huges [9].
A few decades later, the device that preceded the first biosensor was introduced in 1956 by Leland C. Clark. As an expert in by-pass surgeries, he realized the need for an oxygen detector. Upon observing the degree of redness of the blood after oxygenation, he could adjust the oxygen levels in the process to attain a desired degree of redness. Consequently, he also achieved the right degree of oxygenation. By then, it was known that oxygen could be reduced at a platinum electrode, which marks the advent of the oxygen electrode. In order to calibrate the oxygen electrode, Clark added small amounts of glucose as a substrate for glucoseoxidase to deoxygenate the test solution. The mechanism consisted in removing oxygen by converting it to hydrogen peroxide. Clark noticed that it could be used to sense glucose, and built the first named biosensor in 1962, and the biosensing technologies have seen a massive growth since [10]. The emergence and rapid growth of the biosensor field resulted in the creation of a dedicated journal on the subject, *Biosensors and Bioeletronics*, in 1985. By 2011, it had published roughly 10% of the papers ever printed on the matter [11]. After its implementation in medical sciences, the concept of biosensing was extended to a wide range of areas including environmental monitoring, management of water, agriculture, food quality and soil analyses [1].

Most known biosensor is the glucose sensor that assess glucose levels in diabetic patients. It was widely studied the glucose quantitative monitoring in blood because of its importante impact on reducing the risks of diabetes mellitusinduced heart diseases, kidney failure and blindness [12]. Recently innovative technologies were developed in medical field as smartphone based analytical biosensors for patients that were developed for such as blood cholesterol, uric acid, blood lipid and β-Ketone monitoring outside a clinical laboratory [13–15]. A biosensor is a device that can detect a biological or chemical reaction by generating an electrical signal proportional to the concentration of the analyte in the reaction [1]. Biosensors are implemented in industries such as medical, food, eviornment. A biosensor is made of:

- Analyte : Target molecules one wants to detect (e.g. enzyme detection, the enzyme is the analyte).
- Bioreceptor : Design molecule that recognises the analyte, some examples of bioreceptors are enzymes, cells, aptamers, deoxyribonucleic acid (DNA) and antibodies.
- Transducer : Is the element that converts the bio-recognition into electrical or optical signal that are proportional to the amount of analyte.
- Electronics : The part that is responsible for processing the transduced signal and prepars it for display.

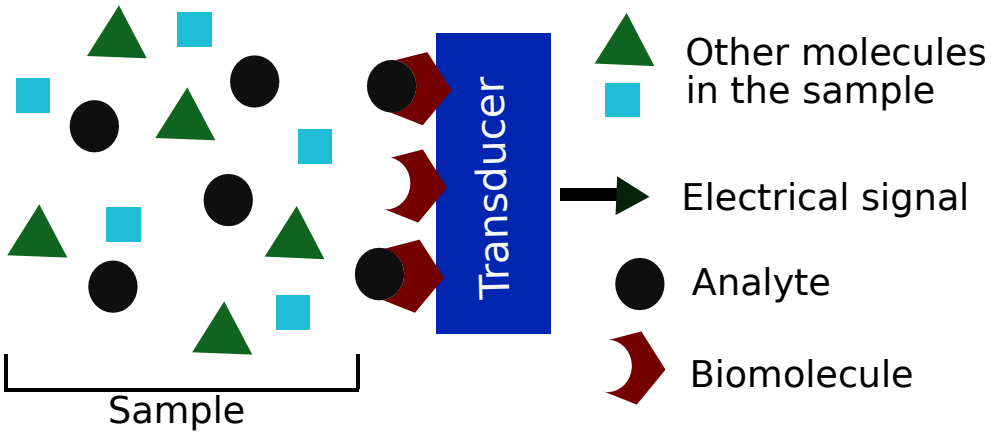

Figure 2.1: Fundamental units of a biosensor. Figure adapted from [16]

Figure 2.1 schematically depicts a biosensor and how each part works as described above. A sample is available and put in contact with the transducer, the designed biomolecule that detects the analyte binds to it and the electrical signal changes.
There are four distinct types of systems depending on the signal being transduced [16]: electrochemical [17], optical [18], piezoelectric [19], and thermal [20] as is possible to see in Figure 2.2. The most successful optical biosensor is the glucose analysis of blood

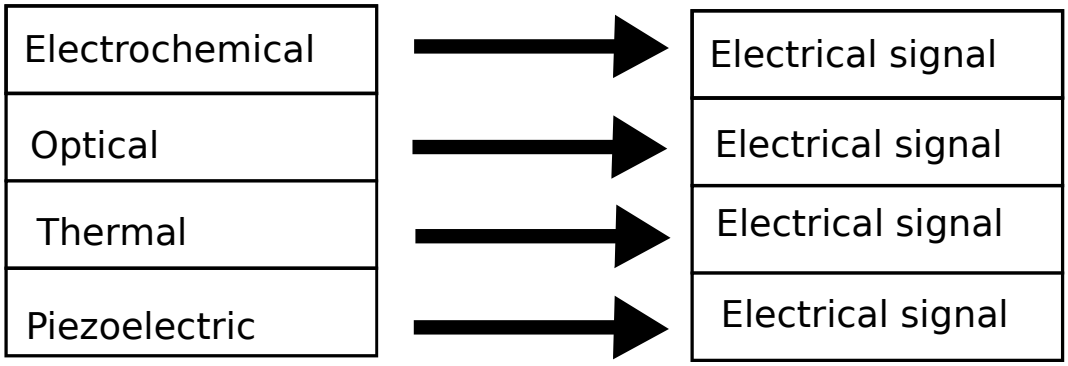

Figure 2.2: Types of biosensors depending on transduced signal. Figure reproduced from [16]

that diabetic patients use to monitor glucose levels. Optical biosensors also work with biomolecules such as enzyme, antibody, protein, nucleic acid or cells. This bioreceptor interact with the analyte, a light source illuminates the sample the interaction leads to a change in the light wave and the transducer displays it. One of the most known optical sensing technologies is surface plasmon resonance (SPR), that can be observeed in Figure 2.3 this phenomenon occurs on metal surface at the interfaces of two media, when illuminated by polarised light at a specific and known angle, generates a surface plasmons and consequently a reduction of intensity of reflected light, the angle is known as resonance angle. The effect is proportional to the surface mass, when there is interaction between analyte and biomolecule the surface mass increases and that causes an angle shift that can be measured [18].

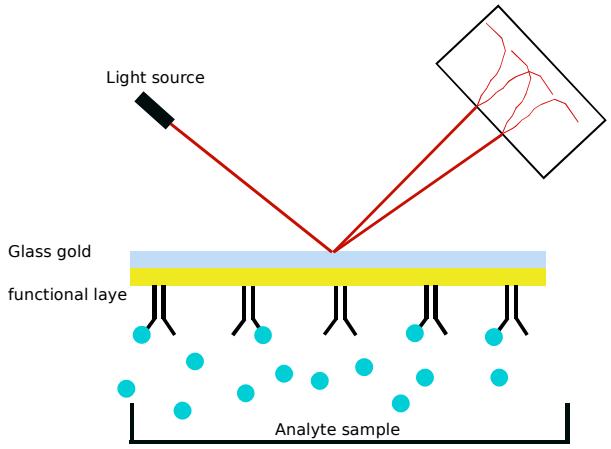

Figure 2.3: SPR biosensor. Figure adapted from [18]

Many of analyte-biomolecule reaction are exothermic, this make possible to identify a presence of the analyte. The biochemical reaction usually involves specific enzymes for specific substrate, the turnover rates of the exothermic reaction are often rapid. Enthalpy changes are measured. Usually uses an immobilised enzyme reactor, with differential temperature measurements. A pair of thermal transducers are positioned across the enzyme column, the thermal signal becomes proportional to the analyte concentration [20].
Piezoelectric platform or crystal is a sensor that works on the principle of oscillations change due to a mass bound on piezoelectric crystal surface. This is a physical phenomenon related with the ability of a material to produce voltage when mechanically stressed. There is a type of crystal names asymptotic crystals that does not have center of symmetry, that show piezoelectricity. Some examples are quartz, aluminium phosphate, aluminium nitride and others. These materials are the base of this type of sensors. The sensor is excited by alternating voltage given on the crystal surface by two electrodes, this alternating voltage causes oscillations on the crystal and the frequency of this oscillations is measured, when the analyte bond to the electrode on crystal surface the frequency changes and thas change can be measured [19].
Electrochemical biosensors are related with a chemical interaction between the biomolecule and the analyte, this promotes a change in the electric signal, changes in accordance with analyte concentration. This type of biosensors is subdivided in three, voltametric, potentiomentric and impedimetric.
Voltametric is used to quantify the analyte. A potential is applied onto electrode surface and change in current is measured utilising two or three electrode systems. One working electrode to sense the chemical reaction that takes place on its surface, and a reference electrode to provide a constant reference voltage to circuit. The third electrode can be employed or not, to eliminate the resistance between electrodes and complete the circuit.
Potentiometric biosensor, a constant electric current is applied, a redox reaction strats occurring on the electrode in the presence of the analyte and that generates a potential difference in electrodes. This potential difference is proportional to analyte concentration.
Impedimetric biosensors combines of resistive and capacitative properties of materials, based on perturbation of a system at equilibrium by a small amplitude sinusoidal excitation signal [21]. This kind of biosensor was widely studied because of its high sensitivity and selectivty.
The work presented throughout this thesis is focused on sensing via electrochemical signals measured by impedimetric systems. Impedimetric biosensors field is expanding. It has been studied enzyme based biosensors for collagenase detection where the impedance signal change was caused by proteolytic digestion of gelatin coated interdigitated gold electrodes [22].To investigate integral membrane proteins a system of Peptide-tethered lipid membranes (tBLMs) on gold support were design as biomimetic system. Cytochrome C oxidase (COX) from bovine heart was incorporated into the preformed peptide tBLM. Quality of lipid films and ion transport across them were study with impedance spetroscopy. The author found a poor quality of the peptide-supported lipid monolayer abd

bilayers where the electrode was only partially (70%) covered with a bilayer and approximately 30% with defect domains of a monolayer of peptide or peptide-lipid. This system can be integrated in biosensor application [23]. Other study [24] focused on impedimetric biosensor based on functionalized graphene oxide nanosheets with a high ratio of horseradish peroxidase (HRP) and detection of antibody. For detection of carcynoembryonic antigen (CEA) the authors coupled captured antibody-modified glassy carbon electrode with enzymatic biocatalytic precipitation of 4-chloro-1-naphtol (4-CN). The performance and factors influencing the properties of the impedimetric immunosensor were studied and evaluated. In optimal conditions the results showed the dynamic concentration range of impedimetric immunosensors extended from 1.0 pg mL^{-1} to 80 ng mL^{-1} CEA with a detection limit (LOD) of 64 pg ML^{-1}. Intra-assay coefficient was less than 7.5% and inter-assay coefficient of variation was less than 11%.

Biosensors applied to medical science are widely studied as well and in 2013 was developed an impedimetric immunosensor for a cancer marker detection in brain tissue. As a prognostic marker for brain tumor Murine double minute 2 (MDM2) has been widely studied. In this article the author present a new label free impedimetric immunosensor for detection of this marker. Based on cysteamine self assembled monolayers on a clean polycrystalline Au electrode surface. The self assembly was monitored with cyclic voltametry (CV) and eletrochemical impedance spectroscopy (EIS), using $Fe(CN)_6^{3-/4-}$ solution as a redox probe. The results showed a linear proportionality between the increase in relative electron-transfer resistance and the concentration of MDM2 in the range of 1pg/mL-1μg/mL. the LOD was 0.29 pg/mL in phosphate buffer saline (PBS) and 1.3pg/mL in mouse brain tissue homogenised [25].

A biosensor for human epidermal growth factor receptor-3 (HER-3) quantification was published in 2013 [26], where the authors made use of a gold electrode surface, layered with hexanedithiol, gold nanoparticles and crysteamine by glutaraldehyde. Anti-HER-3 antibody was covalently attached to cysteamine by glutaraldehyde, this was the innovative step where the last, was used for the first time as a bioreceptor in a biosensor. Gold electrodes surface characterization was obtained by means of electrochemical impedance spectroscopy and voltammetry during anti-HER-3 immobilization process. Results were a good performance of HER-3 detection ranging from 0.2pg/mL to 1.4pg/mL. EIS studies showed electron transfer resistance decreased more by modification of cysteamine. Amino groups attract the negative charges of the redox probe so the electron transfer resistance decreased. The decreases in peak currents resulted from binding of anti-HER-3 and BSA, appeared as certain increase in charge transfer resistances as expected, due to insulating properties of anti-HER-3 and BSA.

DNA enzyme functionalized for prostate-specific antigen (PSA) using impedimetric immunosensor was published in 2014. In this studied a higly sensitive and selective impedimetric immunosensor is design for PSA detection with anti-PSA antibody and DNA enzyme-funtionalized gold-palladium hybrid nanotags. Under optimal conditions the dynamic concentration range of the impedimetric immunosensor spanned from 1.0pg/mL

to 50pg/mL PSA with a detection limit of 0.73pg/mL [27].
Electrochemcial impedance spectroscopy is a method widely used because of its high sensitivity and label free electrochemical technique for monitoring bio recognition events at the electrode surface.
As described the different biosensors have different ways to operate and depend on different sources of signal, also each one has its own characteristics that can were summarised in Tabel 2.1

Table 2.1: Biosensing technology summury

Parameter	Electrochemical	Optical	Thermal	Piezoelectric
Technology	Chemical signal [16].	Light signal [28].	Thermal signal [29].	Mass change [29].
Analyte	Glucose, hydrogen peroxide, Sulfide, uric acid, choline, etc. [16].	Biological analytes and analysis of biomolecular interactions [30]	Enymes, ions [29].	pathogens, gases, pesticides, hormones [29].
Industry	pharmaceutical, clinical, military, food [16].	Diagnostic and pharmaceutical [31].	Food, pharmaceutical, cosmetic [29].	Food, pharmaceutical [29].
Advantages	simple, portable, short response time, sensitive, low cost, specific and selective,less amount of sample under inspection [16].	Real-time analytical technology [30].	-	considered the most sensitive sensor [29].
Disadvantages	-	-	Not sensitive to optical and electrochemical properties of the sample [29].	-

2.2 DNA biophysics

Deoxyribonucleic acid (DNA) is the molecule responsible of carrying genetic information in biological cells. It is a polymer composed by monomer named nucleotides. Each of it contains a phosphate group, a sugar group (deoxyribose) and a nitrogen base. The four existent nitrogen bases are adenine (A), thymine (T), guanine (G) and cytosine (C) [32]. The two DNA strands can self assembly through hybridisation of the complementary strands. The two strands run in opposite orientation, from 5-prime (5') to 3-prime (3´) direction as shown in Figure 2.4. DNA is known for its double helix structure discover by Watson a Crick in 1953 [33], it can also create other structures such as single stranded DNA or fold into other inter and intra- -molecular structures [34].

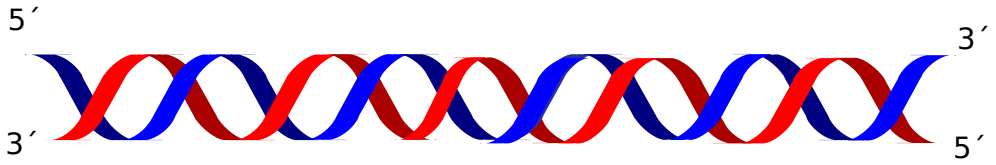

Figure 2.4: Double helix structure of DNA

The four bases have a specific interaction adenine with thymine bind through two hydrogen bonds and cytosine with guanine through three hydrogen bonds. This allows the DNA to have high selectivity because it will just bind with the correct base sequenced strand, as is possible to see on Figure 2.5.

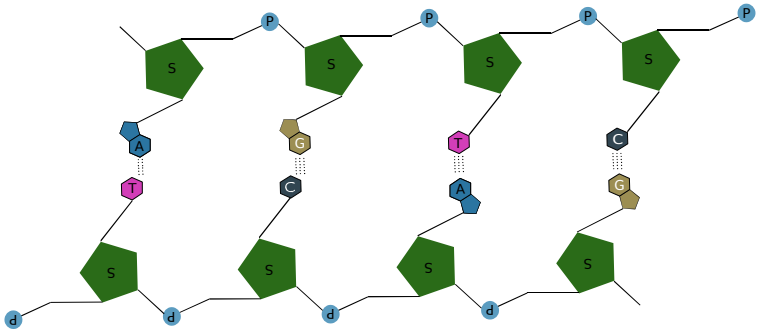

Figure 2.5: Schematic of DNA Structure: DNA chemical structure, each nucleotide linked to its complementary.

DNA hybridisation occurs when two complementary bases are near by and bind creating a double stranded DNA from two single stranded DNA strands. Is a technique used to compare similarity between two species.
The DNA hybridisation thermodynamics have been characterised in the past decades, this allowed to predict DNA behaviour and therefore its structure at nanoscale. SantaLucia Nearest Neighbour model, is used to predict thermodynamics of the binding between oligonucleotides. This was developed with empirical measurements of hybridisation free energies of a variety of DNA motifs [35]

$$\Delta G = \Delta G_{initial} + \sum_{i=1}^{N+1} [\Delta G(N_i, N_{i+1})] \tag{2.1}$$

$\Delta G_{initial}$ is the energy penalty for the initiation and termination of duplexes with an A-T pair. Is also quantitatively predictable the sequence design and their interactions [36], where the free energy for two strands is

$$\Delta G_{Hyb} = \Delta H_{Hyb} - T\Delta S_{Hyb} \tag{2.2}$$

Δ G_{Hyb} is the free energy of hybridisation, Δ H_{Hyb} is the enthalpy of hybridisation, and Δ S_{Hyb} is the entropy of hybridisation.
Assuming, based on empirical observations, that ΔH_{Hyb} $and \Delta$ S_{Hyb} are temperature independent Δ G_{Hyb} is proportional to temperature, which implies that DNA duplexes are less favourable as temperature increases due to the entropic contributions overcoming the enthalpic favourable interactions between the base pairs. As consequence double stranded DNA concentration decreases with increasing of temperature due to duplex de-natoration.
The temperature which 50% of the double-stranded DNA has denaturated to single-stranded DNA is called melting temperature (T_m). This temperature can be known heating the sample followed by a cooling and absorbance analysis show a sigmoidal curve where the middle point gives the T_m. T_m tell how stable the hybridisation for that complex is at room temperature, as far as the T_m is from room temperature as stable is the structure. So hybridisation of DNA strands is considered as second-order reversible reaction in which a strand A and a strand B can self-assemble through sequence-specific interactions as

$$A + B \underset{k_{off}}{\overset{k_{on}}{\rightleftharpoons}} AB \tag{2.3}$$

k_{on} and k_{off} are hybridisation and de-hybridisation constants, and the equilibrium constant can be calculated

$$K_{eq} = \frac{[AB]}{[A][B]} = \frac{k_{on}}{k_{off}} \tag{2.4}$$

Synthetic DNA can be design to build nanometer-scaled structures, to do it there are two approaches, 'top-down' and 'bottom-up'. The first starts from large structures and reduce sizes to the required dimension and pattern by means of an external assembly tool. The bottom-up approach take advantage of internal information of molecules to guide their autonomous self-assembly into nanostructures. Molecular self-assembly has create numerous examples of symmetric or periodic structures with extremely organised features. It is in this field that DNA-based assembly has transformed nanoscience.
DNA nanotechnology is an example of bottom-up fabrication [37] that exploit the physical and chemical properties of the DNA molecule. It have been being developed in the last thirty years and had fast development [38]. These structures can be integrated in systems with other technologies, they can be design to build crystals, 2D and 3D lattices [39]. Molecular self-assembly offers possibility of control 3D structures with nanometer precision [40].
Crystals can be assembled using predictable interaction. 2D crystals can be obtained by autonomously growing by self assembly of tiny beats of single stranded DNA (ssDNA) called sticky ends in DNA tiles such as double-crossover (DX), this molecules are the DNA [37, 40],Figure 2.6 shows two types of DNA nanotechnology tiles. More recently

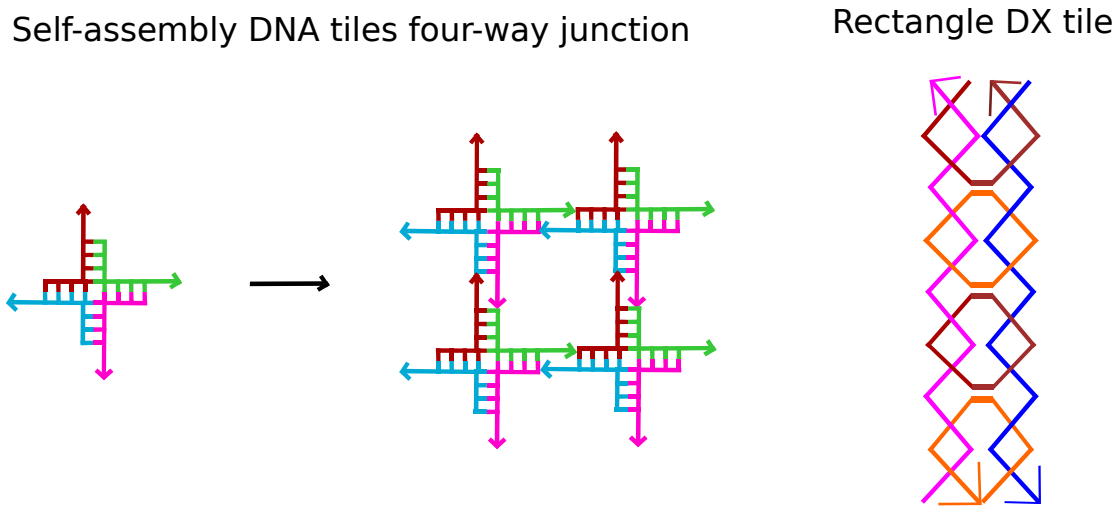

Figure 2.6: Two examples of DNA nanotechnology tiles. Figure adapted from [37]

in 2006 Paul Rothemund [41] published a method for DNA construction based on viral scaffold single strand of DNA that folds into itself into a desired pattern, this is called

DNA origami, where based on DNA molecules patterns is possible to create images like maps, smiley faces or shapes [41].
DNA is also integrated in biosensors and is a very used molecule to target analytes.
Fluoroquinolones (FQs) detection is important in food and environment industry. An eletrochemical sensing system was developed for highly sensitive and specific, using single-stranded DNA-binding protein (ssB) as barrier for the access of redox probe $[Fe(CN)_6]^{3-/4-}$ to the surface of gold electrode [42]. This system showed to need less than one hour to detect ciprofloxacin, and in absence of it the ssB interacts with aptamer blocking the access of redox probe which results in a weaker current signal. This study showed a LOD of 263pM for ciprofloxacin, this system was tested in serum, milk and water with LOD of 336, 351 and 261 pM respectively.
Streptomicyn is sensible in a system based on exonuclease (Exo I), wihch complementary strand (CS) of aptamer arch-shape structure of aptamer (Apt)-CS conjugate gold electrode. The Arch-shape stucture of Apt-CS conjugate to acts as a gate and barrier for the access of the redox probe to the surface of the electrode, Exo I has the function on digesting the single-stranded DNA (ssDNA). When the system does not have streptomicyn the 'gate' remains closed, consequently the electrochemical signal e weak. when streptomicyn is added to the system the the Apt-CS breaks and Apt bind with streptomicyn and the arch-shape structure is disassembled and the electrical signal increases. This work had a LOD of 11.4 nM this method was tested in milk and serum and the LODs preformed were 14.2 and 15.3 nM respectively [43] Tetracyline (TET) is also detectable by a design aptasensor system. Electrochemical impedance spetroscopy showed a linear relation between logarithm of tetracyline concentration and and the charge transferred resistance. with a LOD of 1 ng/mL counting on 15 minutes detection. Using gold electrodes the aptasensor was linked to the electrode and blocking the way to the redox probe $[Fe(CN)_6]^{3-/4-}$ in absence of TET, once TET was added the aptasensor likes to TET and the changing in shape opens space to the probe to contact with electrode and the signal measured changes. Also experiments in milk were preformed showing good results of recovering of 90-97% [44].
DNA nanotechnology can have many applications, and the possibility of predict it behaviour opens the possibility to create controlled systems and integrate DNA nanotechnology in adhesion systems such as vesicles. Aside from DNA vesicles can be functionalized with other molecules, to functionalize a wide kind of structures as mentioned before, this anchor system is represented in Figure 2.7, in this figure is possible to see a cholesterol anchored DNA double stranded. It can be sensitive to its complementary strand and that the most easy an cheap way to try a system but can also be design to sense other molecules, this DNA sensors are named aptamer. As mentioned in the previous Chapter 1, DNA was also used to sense proteins being part of a vesicles adhesion system. The study previously mentioned on sensitivity of analyte concentration [8]. Streptavidin was the analyte and at low concentration adhesion little occur, with the concentration increasing it starts increasing the adhesion events and at high concentration each strand has its own molecule

having no need to adhere to each other. A study proved that temperature is an adhesion dependent factor, at low temperatures the vesicles were rigid and with less deformable ability the adhesion did not occurred so easily, on the other hand at high temperatures vesicles show to be highly deformable and able to change shape and enable the adhesion to happen at nearly all the surface [6]. In both cases the interaction came from a sticky end DNA system where a single stranded DNA complementary to other automatically hybridise. All vesicles were functionalized with the two spices and so could happen a bridge-like conformation if the binding happens between two strands in different vesicles or loop-like in case of the strands stick to strands in the same vesicle. But there are other kind of interaction involving DNA that can mediate cell adhesion such as phospholipid interaction with DNA. 2-Methacryloyloxyethyl phospohorycholine (MPC) can interact with DNA in the presence of Ca^{2+} ions [45]. A lot of work can be done regarding the technologies addressed in this chapter. DNA mediated vesicles adhesion is a technology to develop with a lot of potential. In this point biosensing can benefit with this integrating different works that can be join and are compatible together.

Figure 2.7: Cholesterol anchored DNA

2.3 Vesicles adhesion

Membranes can be made of phospholipids, sphingolipids and sterols. Phospholipids have a hydrophilic phosphate head and two hydrophobic acyl chains. Because of this structure the behaviour is different in aqueous or organic media in presence of water, due its steric hindrance, ionic repulsive forces and hydrophobic association phopholipids arrange in micelles or bilayers structures shown in Figure 2.8. Cells membrane is made of lipid bilayer. Cells attractive interact with each other, a is seen the body tissues. But this lipid membranes can be created artificially and the membrane can have the same function as a cell. Lipid vesicles are used for a wide kind of applications such as drug delivery [46], sensing agents [47] and microreactors [48]. This is due to its capacity of mimicking cells tissues and behaviours without having biological activity to disturb the systems. Lipid vesicles can be functionalized with DNA, antibodies, tethered small molecules, nanoparticles, and others. This characteristic gives it the possibility of being in the base of self-assembly systems by ligand/receptor multivalent interactions. These membranes are lipid bilayers, Figure 2.8, composed by phospholipids and can be mono- or polilipid, which means that the membrane composition can have one ore more lipids in its constitution, also it often includes other molecules than phospholipids that helps strengthen

and adjust membrane characteristics relative to interaction with other molecules such as permeability one example of this is cholesterol, that is very common to be part of membranes. Another advantage of cholesterol being part of the membrane is because it can be used as an anchor to functionalize lipid membranes.

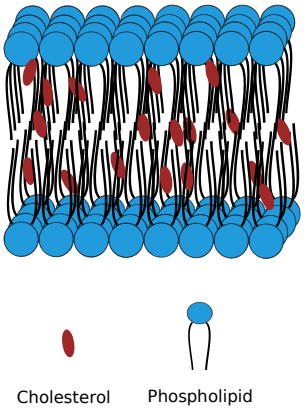

Figure 2.8: Lipid bilayer

Vesicles adhesion mediated by DNA strands is one popular way of mimicking cell-to-cell interactions, using the programmability and predictability of DNA Nanotechnolog, as represented in Figure 2.9 the vesicles adhesion is mediated by DNA complementary strands that make the bridge, in this specific case the bridge is made of sticky end DNA. DNA can be design to be sensitive to different kind of molecules, which enables to conjugate adhesion with biosensing. If the DNA is sensitive to a specific analyte and that analyte is in solution, that will trigger the adhesion and that can be detected measuring the resistance promoted by the media before and after adhesion. General impedance can be measured when applied an AC current and if the change in the signal is measurable that is an indication of analytes' presence.

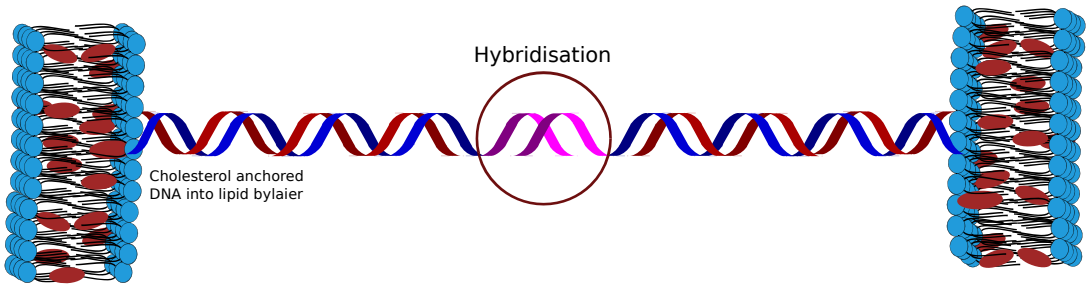

Figure 2.9: Membrane adhesion mediated by sticky end DNA.Figure adapted from [6]

2.4 Theoretical Concept of Impedance

In a presence of a alternate current (AC), the resistance of a media presents magnitude and phase. Ohms law, $V = IR$ gives the relation of voltage (V) depending on current (I) and resistance (R). This equation can also be written as $Z = \frac{V}{I}$, this ratio is known as impedance (Z), which represent a general concept of resistance. Because it occurs in the presence of an AC current it can be represented as sinusoidal, this gives the phase property.
Impedance is a property of resistor, capacitor or inductor. Depending on which one it is being measured it has different expressions. Considering a resistor, $V = IR$ and $I = e^{+j\omega t}$, $e^{+j\omega t}$ is a imaginary rotative vector, where j is imaginary unit of the vector, ω is the frequency and t is time [49].

$$V = Re^{+j\omega t} \tag{2.5}$$

$$\frac{V}{I} = \frac{Re^{+j\omega t}}{e^{+j\omega t}} \tag{2.6}$$

$$\frac{V}{I} = R \tag{2.7}$$

$$Z = R \tag{2.8}$$

In the case of an inductor (L) by defenition $V = L\frac{di}{dt}$, if one consider $I = e^{+j\omega t}$, is possible to make the same procedure again [49].

$$V = L\frac{d}{dt}e^{+j\omega t} \tag{2.9}$$

$$V = j\omega Le^{+j\omega t} \tag{2.10}$$

As mentioned before $Z = V/I$, if V in 2.6 is divided by I, in this case the result will be:

$$V = \frac{j\omega Le^{+j\omega t}}{e^{+j\omega t}} \tag{2.11}$$

Terms $e^{+j\omega t}$ cancel and the result is 2.13.

$$\frac{V}{I} = j\omega L \tag{2.12}$$

$$Z = j\omega L \tag{2.13}$$

In capacitors (C) $I = C\frac{dv}{dt}$ and $V = e^{j\omega t}$. In the same way impedance expression for capacitor can be calculated. [49]

$$I = C\frac{d}{dt}e^{j\omega t} \tag{2.14}$$

$$I = j\omega C e^{j\omega t} \tag{2.15}$$

$$\frac{V}{I} = \frac{e^{j\omega t}}{j\omega C e^{j\omega t}} \tag{2.16}$$

$$Z = \frac{1}{j\omega C} \tag{2.17}$$

In presence of media that offers resistance to the electric field is possible to measure impedance and variations in this signal can be obtained with change on resistance of the media. Electrolytes are ionic liquids that present good conductivity (σ), this means that they can conduct electric current trough them. Conductivity is the inverse of resistivity (ρ), accordingly with the material being more or less conductive it presents resistivity to the current as well. This conductivity is related with the concentration of ions in solution. Ions are responsible for the electric field conductance through the media.
There are strong electrolytes, which dissociation is complete unless the concentration is too high, and weak electrolyte that has low dissociation constant and the reaction can occur in both ways, products and reagents. For high concentrations of ions the conductivity has a limit, where the dissociation of the ions stop happening because of saturation of the media due to excess of ions in solution.
Resistance (R) can be calculated for regular geometries similar to Figure 2.10 of homogeneous material with section A and thickness L through $R = \rho\frac{L}{A}$, ρ is resistivity of the media, L is the distance between the two electrodes and A is the surface area of the electrode. According to Kohlrausch's law of independent migration of ions strong electrolytes resistivity is $\rho = \Lambda_m - k\sqrt{C}$, where Λ_m is the solution conductivity, k is Kohlrausch constant for that ion [50]. joining this two notions:

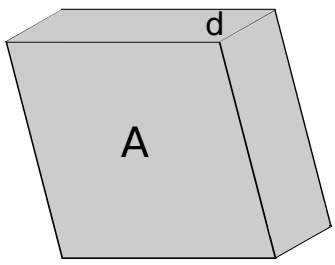

Figure 2.10: Regular geometry: Is applicable the resistance equation $R = \rho\frac{L}{A}$, with area (A) and thickness (d). In case in electrolytes because they are liquids the area corresponds to electrode area a thickness is the distance between the electrodes, where the electrolyte is placed.

$$R = \frac{1}{\Lambda_m - k\sqrt{C}} \frac{L}{A} \tag{2.18}$$

Λ_m can be calculated from ionic conductivity (Λ_{m0}) multiplied by concentration (C). The final given equation of resistance in the presence of electrolyte media is 2.19:

$$R = \frac{1}{\Lambda_{m0} C - k\sqrt{C^3}} \frac{L}{A} \tag{2.19}$$

With the increasing interest on this kind of technology new approaches came up and one of the most used technologies are microfluidics. Microfluidics are small systems that can be very complex and designed for the most diverse kind of applications. It enables the manipulation of fluids on the microscale level, its dimensions have often less than 1 mm. This tecnology has the advantage of scaling many physical laws as rapid diffusion, laminar flow, rapid thermal trasnport and take advantage on the large surface related to the volume. Many tecniques of fabrication have been developed although the most common is soft lithography, introduced in 1998 [51]. This method has a need of a clean room which is expensive and time consuming. This made engineers invest time in developing other ways to produce microfluidics. The last can be produced using wide range of materials and techniques, such as polymer laminates and 3D printing. Microfluidics are very useful in biosensing because of allowing controled systems with small volume of sample, less than picolitres [52]. Integration of microfluidics in biosensog offers new opportunities for future biosensing applications such as portability, real-time detection, increased sensitivity and selectivity and also analysis of more than one analyte in the same device [53]. Lab-on-a-chip (LOC) concept arises from trying to integrate laboratory analysis in a microfluidic device, this kind of devices are usually ranging around square millimetres.

Chapter 3

Materials and Methods

3.1 Vesicle Preparation

3.1.1 Electroformation

Giant unilamellar vesicles (GUV) were prepared by electroformation. A volume of 45 μL of the pre-preparated mixture with 1,2-Dioleoyl-sn-glycero-3-phosphocholin (DOPC) at 4 mg/mL in chloroform and texas red (TR-DHPE) in a molar ratio of 0.008 is spread over a conductive side of an Indium tin oxide (ITO) slide until is obtained a dry film of lipid. Texas red is a fluorescent dye that enable the vesicles observation at fluorescent illumination in the microscope the brightness intensity can be measured to comprove adhesion. This slide is placed on the dessicator for one hour in the dark, because TR is photosensible, afterwards the slide with lipid is assembled with other ITO slide spaced by a 1 mm Polydimethylsiloxane (PDMS) spacer, represented in Figure 3.1. This chamber is filled with pre-degased 300 mM sucrose solution in miliq water. An AC current is applied in the chamber of 10 Hz during two hours, for growth stage and 2 Hz during 1 hour for detachment of the vesicles from the ITO slide, experimental set-up can be seen in Figures 3.2and 3.3 [54, 55].

3.1.2 Vesicles functionalization with DNA

Vesicles were functionalized with DNA nanostructures that will mediate the adhesion, described below in Section 4.2. The DNA is diluted from 7 μM to 0.2 μM in 10 mM Tris + 100 mM NaCl buffer. The vesicles are mixed with the DNA constructs using an iso-osmolar buffer with 11,6 mM Tris + 116 mM NaCl + 82.5 mM Glucose. Glucose is used to harness the density mismatch with the inner buffer (sucrose) and promote sinking with gravity. This is desirable for imaging, and it also exploited in the microfluidic design to

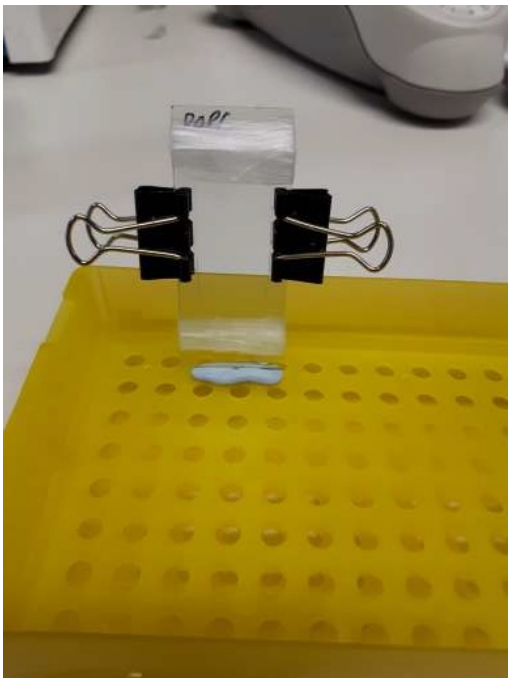

Figure 3.1: Electroformation chamber: Two ITO slides, two clamps on the sides to close and press to prevent any leak from the sides and parafilm on bottom and top also to prevent leakage.

Figure 3.2: Electroformation chamber connected to electrodes.

Figure 3.3: Electroformation set-up

accumulate vesicles in the chamber. The vesicles are functionalzed with both constructs A and B respectively represented in Figure 3.4 in a saturated density state, to saturat the surface concentration of linkers on the GUVs. Upon mixing 345 μL of the last buffer, 50 μL of each DNA construct (A and B) and finally 55.2 μL of GUVs, the vesicles are incubated overnight under rotation.

3.2 Microfluidics

Microfluidics devices are made of PDMS using established photolitograpgy and soft litography techniques. With a negative photo-resist, SU-8 2000, in this work was used SU-8 2050. The 4 inch silicon wafer is cleaned with acetone and isopropanol; heated for 20 minutes to completely dry it and then goes to O_2 plasma cleaning for five minutes to make render the surface more hydrophilic and improve the adhesion between the silicon wafer and the SU-8. The spin-coating program is chosen to achieve a film thickness desired, in this work, devices had 25μm, 70μm, 80μm and 100μm, final devices are 70μm. The design is pre-made in Autocad and imported to a table-top laser direct imaging (LDI) system (LPKF Protolaser LDI, Germany). After laser writing, the wafer is heated to 65 °C for 2 minutes and then 95 °C for 9 minutes, as per datasheet, to complete the cross linking. Once the wafer cools down to room temperature, approximately 20 minutes, is submerged in Propylene glycol monomethyl ether acetate (PGMEA), a photo-resist solvent that is used to wash the SU-8 that was not exposed to the laser. The final result is a mold with negative of the channels. Microfluidic chips are prepared from PDMS by covering the mold with liquid PDMS mixture (1:10 ratio of curing agent), and cooked for 2 hours in the oven at 60ºC. Afterwards, the chips can be individually cut, and holes are punched at the inlets and outlets with 0.7 mm holes to main flux channels and 1.2 mm

hole for electrodes in-let and out-let. The PDMS chip and a glass coverslip are subjected to O2 plasma for 30 seconds and then assembled. The assembled chips are subsequently placed in the oven at 60ºC for 3 minutes. For the electrode deposition [56], the chips are placed on a hot plate at 70 ºC, and a low-temperature molten alloy (InBiSn - 51% Indium, 32,5% Bismuth, 16.5% Tin) wire is inserted in the respective inlet, this has a melting temperature of 55ºC which was calculated by differential scan calorimetry (DSC) in appendix A. The alloy melts in the glass and fills the electrode chamber. Finally, the alloy solidifies upon removing the device from the hot plate.

3.3 DNA Design, Preparation and Analysis

The DNA system presented in this work was designed with Nupack [57], an online tool for DNA design and analyses. That system is comprised by two constructs, A and B, and one linker. Each construct is made of three DNA strands. Functionalized strands, which anchor the construct to the lipid bilayer membrane, and either strand A or B. These will have 18 base pairs complementary to the anchor constructs, and also include a 8-basepair domain to recruit the linker. In turn, the linker is 16 base pairs long, containing a domain to bind to A and a domain to bind to B, observed in Figure 3.4. DNA constructs were prepared by annealing over a temperature ramp starting at 95°C at a rate of 0.5°C/min until 4°C/min. Relevant strands (Bb, B_bb, A and Cb, C_bb, B) were mixed stoichiometrically with 100 mM NaCl and 1X Tris.

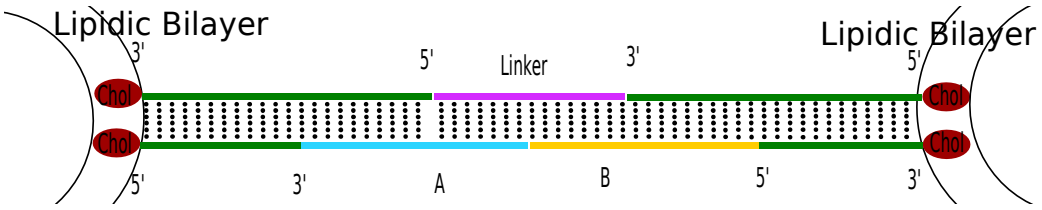

Figure 3.4: DNA system: Lipid bilayer funtionalized with anchored DNA system designed to mediate GUV adhesion: in green, anchoring strands, A and B are complementary to each construct (A to Bb-Bbb and B to Cb-Cbb). The linker is able to hybridize both constructs thereby bridging membranes.

3.3.1 UV-Visible Spectroscopy

Melting temperatures, T_m, were determined through UV-Visible spectroscopy using a Varian Cary 50 UV-Vis spectrophotometer. Samples were prepared by mixing required strands in stoichiometric ratios and diluted such that the total OD_{260} fell between 0.1 and 1. A quartz cuvette was loaded with 700 μL of sample. To prevent evaporation, a small amount of mineral oil was carefully loaded on top of the sample before sealing with a polytetrafluoroethylene (PTFE) stopper. Absorbance was measured continuously

at 260 nm as a temperature ramp was imposed by a Peltier controlled heating block. The two stage ramp consisted of first cooling from 85°C to 15°C followed by a heating step from 15°C to 85°C; both at a rate of 0.2°C min^{-1}.

3.3.2 Agarose Gel Electrophoresis (AGE)

Gels were prepared using agarose at 1.5% (weight) and Tris-borate EDTA (TBE, Sigma-Aldrich - 89 mM Tris-borate, 2 mM EDTA, pH8.3) buffer. The mixture was heated in a microwave in 15-second pulses and swirling in between until the agarose was dissolved completely. SYBR®Safe DNA gel stain (Invitrogen) was added at 0.1% (volume) to the mixture and dissolved gently. The mixture was casted to a thickness of approximately 5 mm and allowed to set for 1 hour. The gel was subsquently transferred to an electrophoresis chamber and covered with TBE buffer. Samples were prepared to contain 750 ng of nucleic acids and brought to appropriate volumes with loading buffer (TriTrack 6x, Thermo Scientific). 20μL of sample were loaded onto the gel along with a DNA ladder (GeneRuler Ultra Low Range, Thermo Scientific). A potential of 75 V (3.75 V cm^{-1}) was applied for 90 minutes, and the gels were subsquently imaged using a GelDoc-It®system containing a UV lamp for illumination.

3.4 Microscopy and impedentiometry set-up

The measurement of impedance in the microfluidic device is done using an analog discovery 2 instrument. This equipment is connected with the electrodes in the device in the microscope to be able to observe the vesicles adhesion as shown in Figure 3.5 and 3.6. The assemble of the impedance measurements set-up is a very sensible step. The electrodes wire is fragile and can break inside the device very easly. The Device must be carefully exposed to electrode objective and connecetd to Analog2 Discover. Also this connection must be done slowly and gently to avoid any damage, because the connection and consequently all the measurements depend entirely on the wires.

The program used with Analog2 Discovery, reprensented in Figure 3.7, is waveform. Both results are displayed at the same time, microscope observations and impedance mesurements. This ways is possible to see what is happening in the system while is possible to see difference in signal measured.

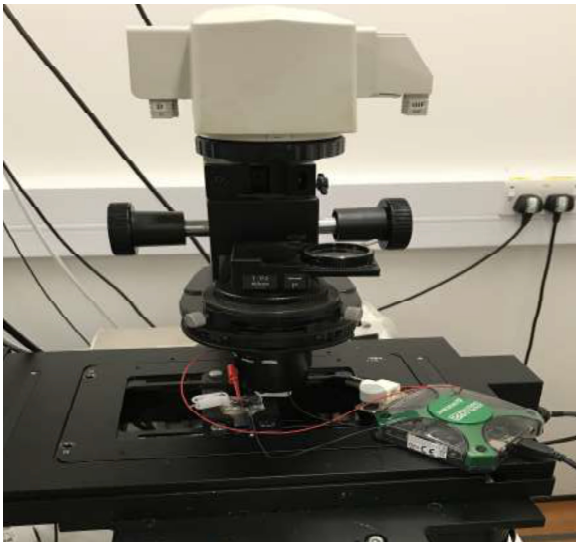

Figure 3.5: Impedimetric measurements set-up: The device is placed in the microscope and connected to the measure equipment.

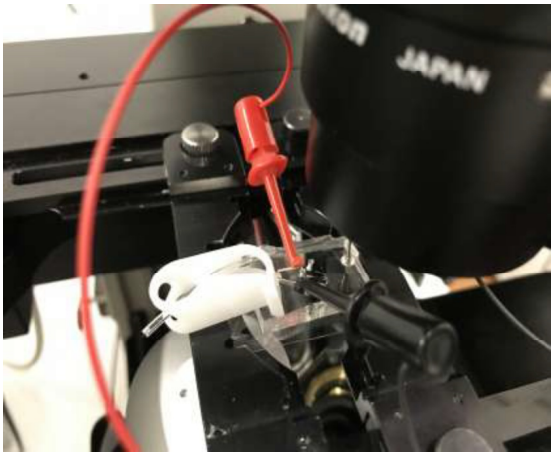

Figure 3.6: Impedance measurements set-up: Device and connected equipment, assembled in the microscope. Closer image of the device and the AC conection. The outlet is clamped with whit clamp, positive electrode is connected to the red wire is the anode and the cathode, the negative electrode is black.

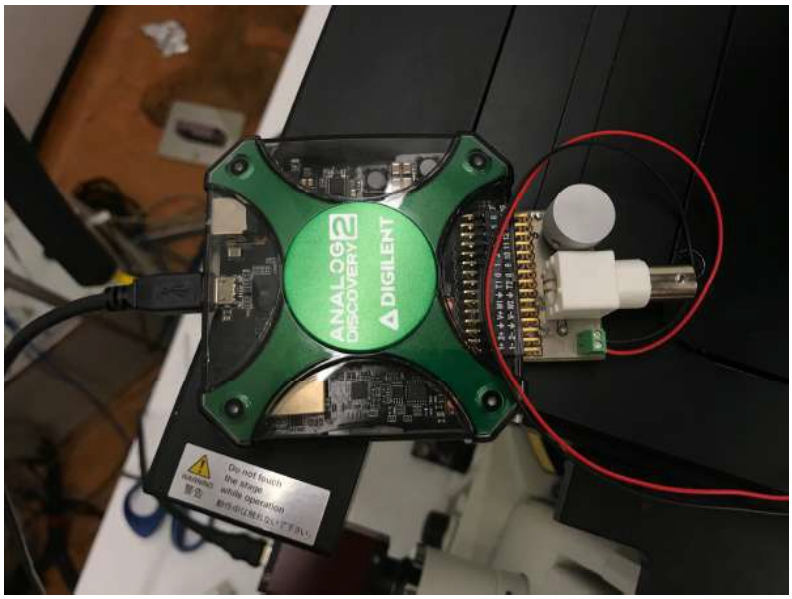

Figure 3.7: Analog Discovery 2: Equipment used for impedance measurements.

Chapter 4

Results

4.1 Microfluidics - Design and optimisation

This work started by developing a microfluidic device. The initial goal was to design a microfluidic device to create a densely packed assembly of GUVs. Microfluidic technology enable working with controlled systems, allowing to flow into the system whatever is wanted to include. In this work is wanted to control the adhesion and measure the impedance difference before and after that step. Microcfluidics enables to create a platform to work in these conditions. GUVs are very flexible, they can be pushed through very small spaces; even GUVs with 50 μm diameter are able to pass through 20 μm spaces. Consequently the design should contemplate this need. Was decided to design a device with a chamber where the GUVs could sink just by gravity. Microfluidic chips were produced in a laser writer by expose a photo-resist to laser that will draw the channels, as described in Materials and Methods section 3.2. This technique implies that the ratio between height and width bust be kept above 0,3 because if not can happen one of two, the SU-8 detaches from the silicon wafer because it does not have enough surface for the height or the development of the SU-8 have the chance of not being well done. The first design was an assembling of all the restrictions, was a chip with two side channels to flow the solution and a chamber in the middle, in line with the inlet to let the GUV sink observed in figure 4.1, Also the microscope image of the SU-8 mold is represented on Figure 4.2.

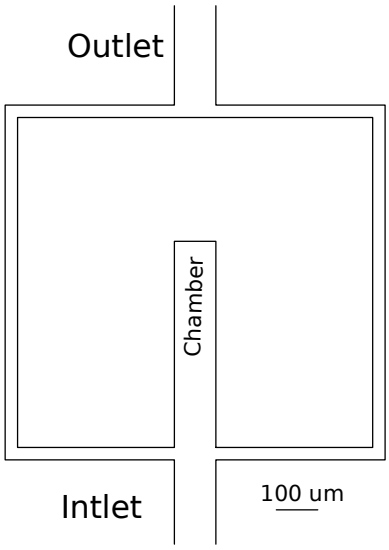

Figure 4.1: Autocad first design: Capacitive design. More information relative to chip sizes in Appendix B

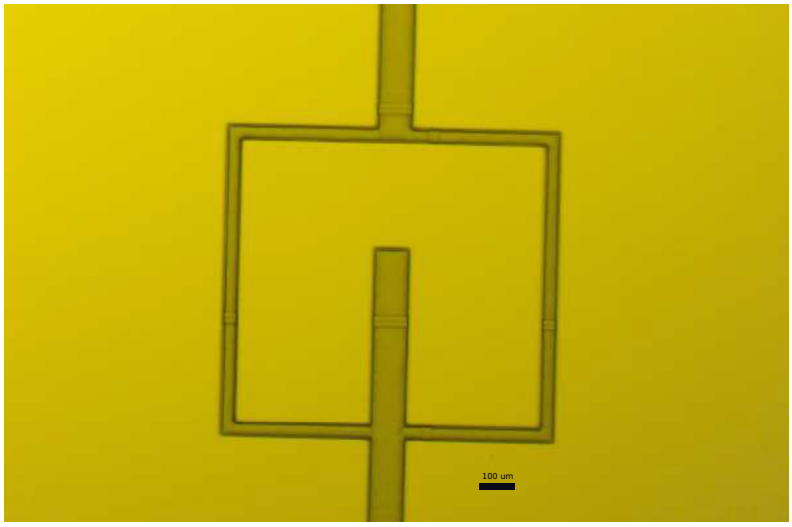

Figure 4.2: SU-8 Channels. First design: Microscope image of SU-8 mold channels. 25 μm heigh, 500 μm chamber length and 100 μm width.

After having the first devices it was flowed BSA to passivate the device and then washed with buffer. Blocked channels were observed as is possible to see in bright field in Figures 4.3 and 4.5, the last image was also imaged in fluorescence in Figure 4.4, where is possible to see that the lipid is passing through but the vesicles burst, that is the reason

to observe a red line and no round shapes. Also the passivating step caused aggregates in the chamber as observed in Figure 4.6. All steps had to be optimised to have a clear chamber to be able to fill the chamber the chip had to be flushed with GUVs suspension, kept it in upward position and wait for 1 hour expecting the GUVs to sink in the chamber by gravity. After repeating this process several times with different dilutions of GUV to buffer such as 1:10, 1:7, 1:5, 1:2 it was observed that the vesicles did not sink in the chamber and they rather flow through side channels and reach the outlet where they tended to accumulate.

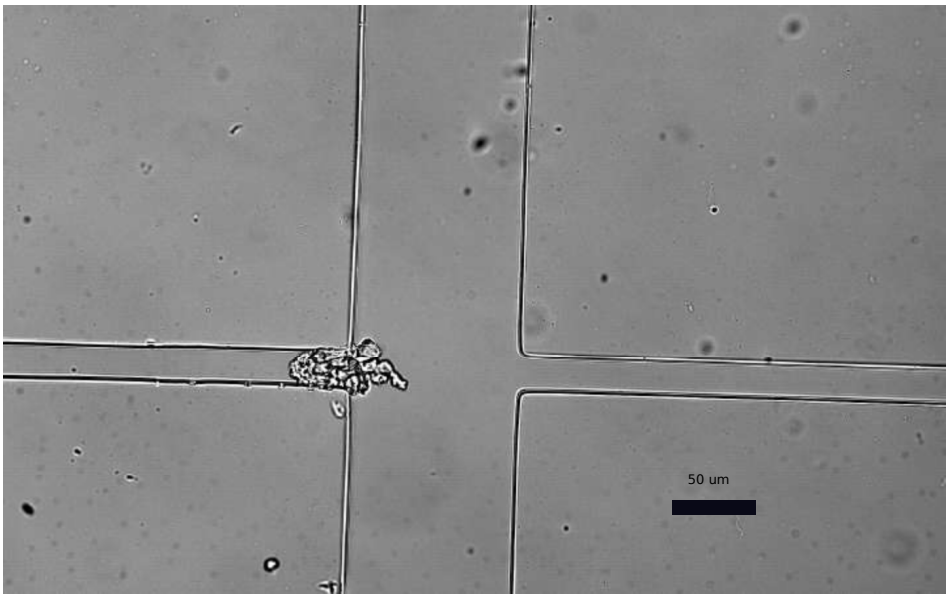

Figure 4.3: Microscope image of chamber and inlet junction. First design: The side channel is blocked. Top of the image is the inlet.

Different designs were used to try a different approach. One channel with pillars to stop the vesicles flow was the second try, shown in Figure 4.7, with just one channel, the vesicles could not flow anywhere else but the main channel where would be measured the impedance. Was also made a combination of the first design integrating pillars, inspired by a paper where the author succeed to enclose packed GUVs [58]. It had three channels and the main channel, wider than the secondary channels, had pillars to stop the vesicles flow presented in Figure 4.7. The two side channels would release the pressure in the vesicles once the flow starts finding hard to pass though the vesicles and pillars. A microscope image of the result of the third design chip is showed in Figure 4.9.

For the last both mentioned, one channel with pillars and three channels with pillars, at microscope observation was possible to see that even with very slow flow rates such as 0.5 μL/hr the vesicles were pushed through the pillars and accumulated in the outlet. This could be a limitation from the syringe pump available because it was not able to flow less than 2.5nL/min, which still very fast and cause high shear on vesicles.
Upon having no results with these designs, it was decided to try the first design but with

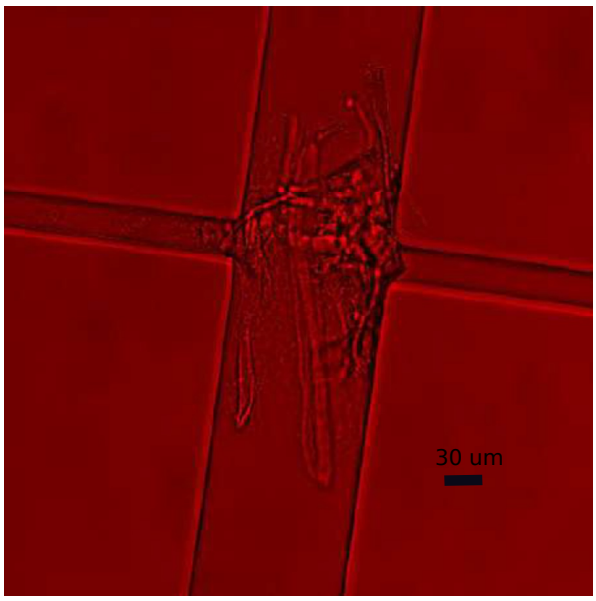

Figure 4.4: Microscope image of chamber and inlet junction 2. First design: The side channel is blocked. Top of the image is the inlet.

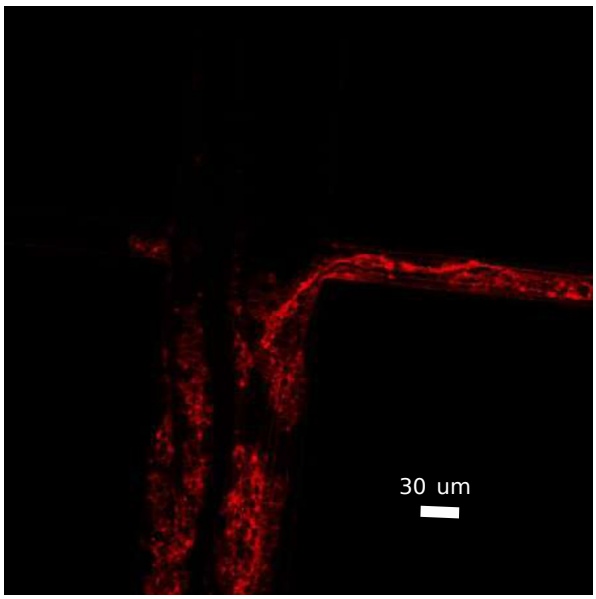

Figure 4.5: Fluorescent microscope image of chamber and inlet junction 2. First design: The side channel is blocked. Top of the image is the inlet.

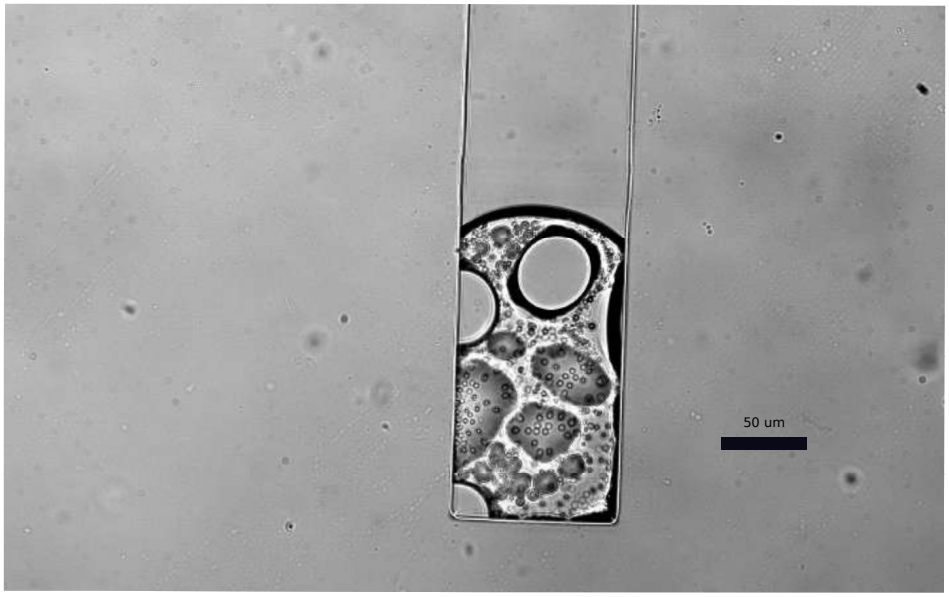

Figure 4.6: Bright field microscope image of chamber. First design: Presence of BSA aggregations, accumulating in the bottom of the chamber. Top of the image is the inlet.

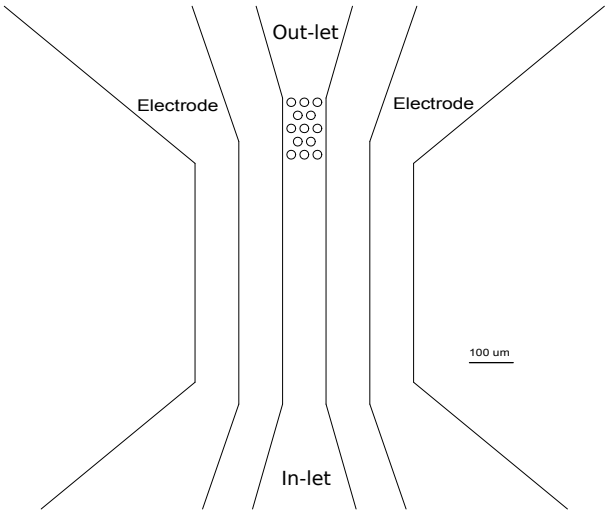

Figure 4.7: Autocad drawing of microfluidic chip, Second design:One way chip with pillars to stop the vesicles flow and allowing the liquid to pass. More information relative to chip sizes in Appendix B

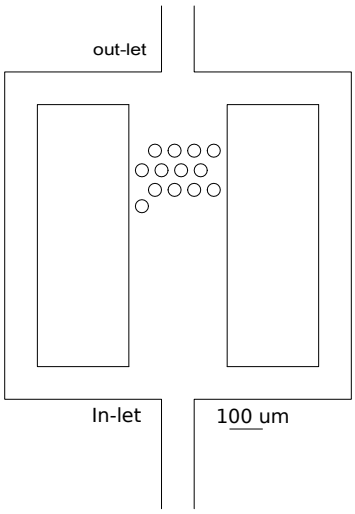

Figure 4.8: Autocad drawing of microfluidic chip, third design: Composed by three channels, the main channel is 300 μm width and is wider to increase the probability of vesicles flowing there, the two side channels work as channel for the liquid to escape and prevent GUVs shear stress and escape through the pillars for excess of pressure. More information relative to chip sizes in Appendix B.

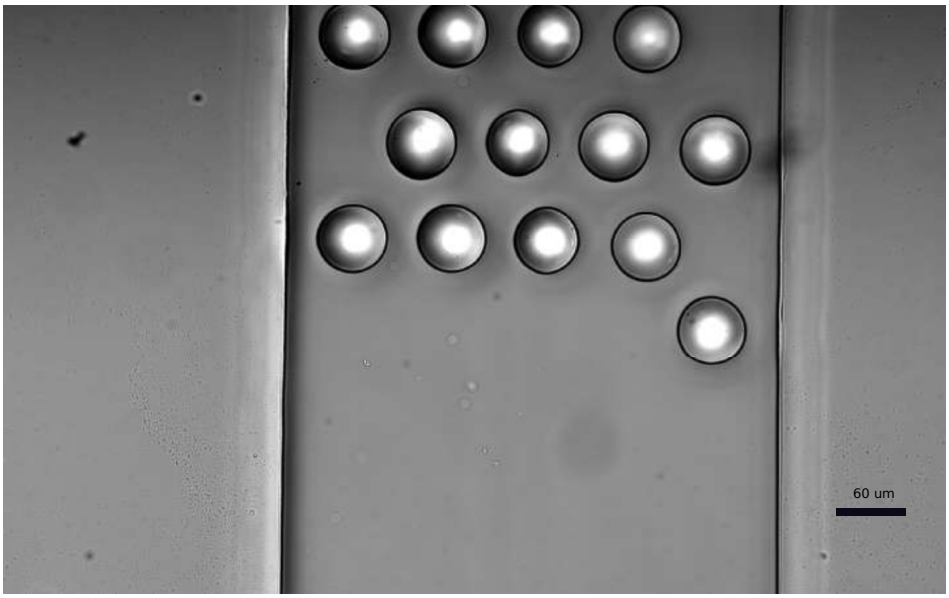

Figure 4.9: Microscope image of the central channel of the third design.

clamped outlet to stop the flow in upward position, because it was observed that there was flow in microscope observations and the GUVs were going with flow through the side channels. In this conditions the GUVs were blocked in the inlet channel and did not sink in the chamber again.
This lead to think that the height of the channels was not enough to enable the GUVs to freely diffuse. GUVs are highly deformable, and this property made it pass through the pillars in the previous designs and caused flow in the GUVs that would not move without flow.
A new mold was made of the same design but with channels 100 μm height . This was the first time it was observed vesicles in the chamber, showed in Figure 4.10 and Figure 4.11. Assuming the designed was now working, electrode integration was attempt. Initially,

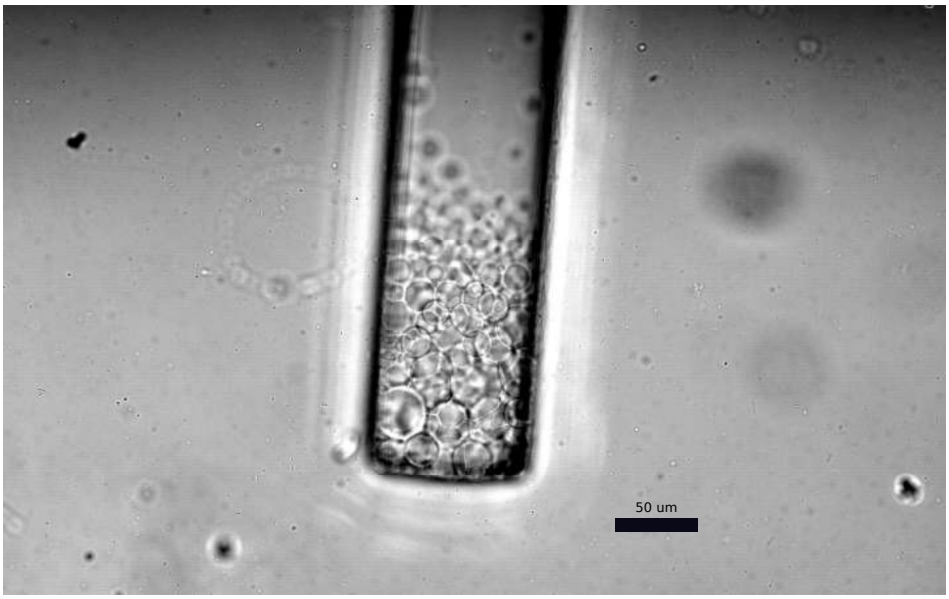

Figure 4.10: Microscope image of microfluidic Chamber: There is a very packed volume of vesicles that fill half the chamber. Inlet is on top

a solution of 3M of NaCl was used in two chambers in each side of the main chamber spaced by PDMS walls of 50 μm. This choice was made to introduce electrodes in a easy way that avoided contact between the electrode and the solution because the buffer used to suspend DNA is usually tris-EDTA and EDTA chelate metals and it changes the chemistry of the solution in a way that we do not know and that can affect the measurements, also the electrode would be damaged and the results would not be reliable.
Electrolytes are conductive and can operate as electrodes when is applied a electric field through it. The design has two parallel electrodes with infinity resistance between, because of its PDMS walls which means the device works as a capacitor represented in Figure 4.12.

Different buffers, with different salt concentrations were flushed in the device to test the reliability of the measurements made in it. Concentrations varied between 50 mM

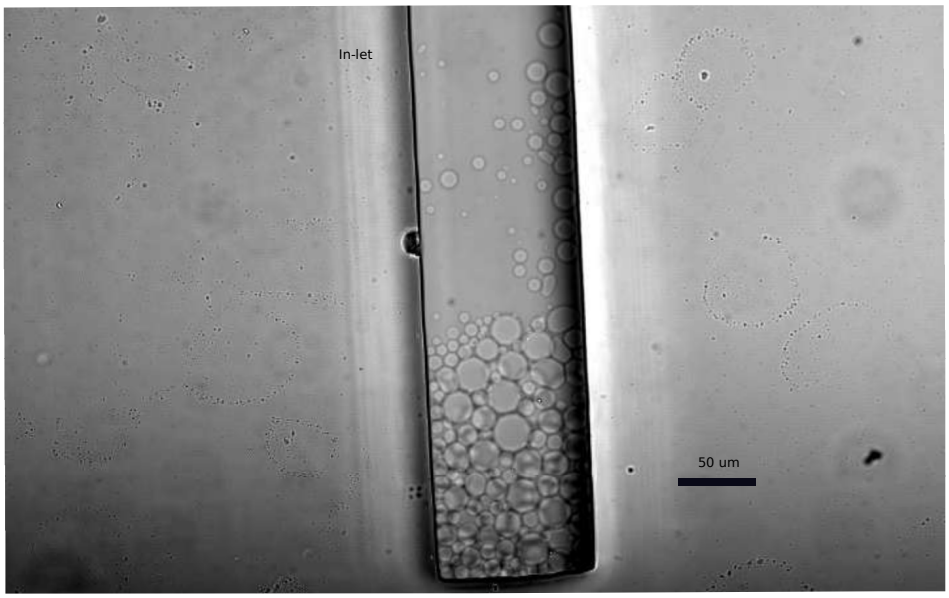

Figure 4.11: Microscope image of Chamber: As in the previous image the chamber is very packed with vesicles with a volume that fills half the chamber.Inlet is on top.

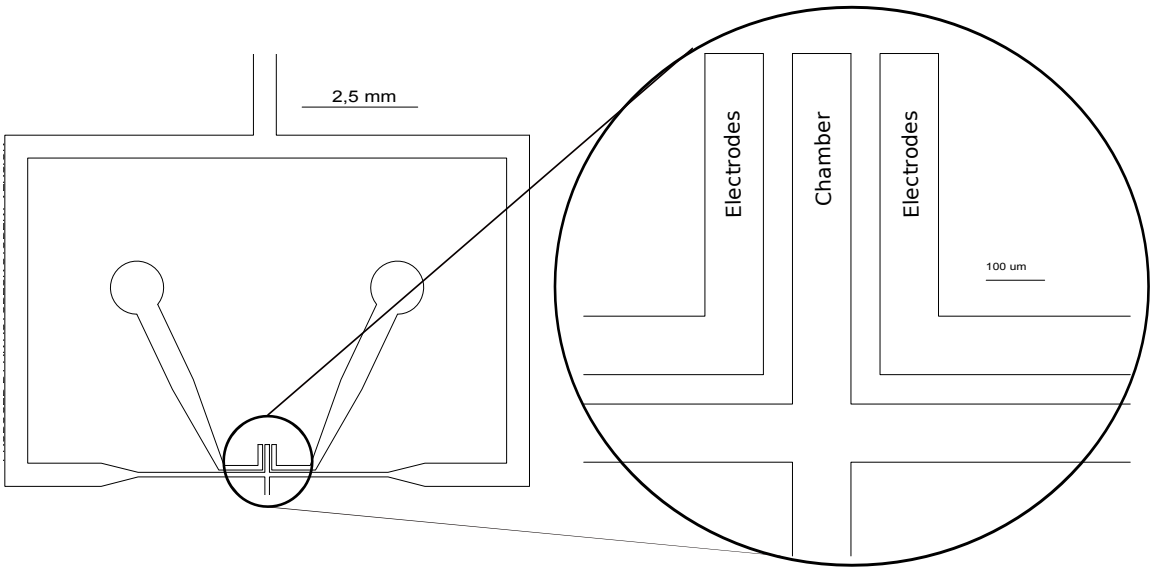

Figure 4.12: Autocad design of microfluidic device with parallel electrolyte electrodes.

and 3M. During the measurements any change was noticed and then it seamed to have no difference in the displayed value with the wires connected or not. To understand why was this happening was calculated the value of capacitance for this design using the equation 4.1, (d) is distance between electrodes, (ε) dielectric constant of the media and A is area of the electrode the result was 35.4 pF. The capacitance of the wires by it self was around 60 F. This was completely out of range and this system had to be redesign.

$$C = \frac{d}{\varepsilon A} \tag{4.1}$$

A new approach had to be done because it was needed that the system could measure either very small values, being very sensible or to increase the signal between the electrodes.

The new design had a similar configuration to the capacitive design, the last one mentioned, but to improve the signal the electrodes are in contact with the GUVs suspension by being part of chamber walls.

The electrodes are integrated in the device after the PDMS is sticked to cover slip. The edge of the chamber is made of 70 μm pillars spaced by 70 μm, figure 4.13. In this case because there is a conductive medium between electrodes, the effect of impedance come mostly from the resistance of the media and so for this design, $Z = R$.

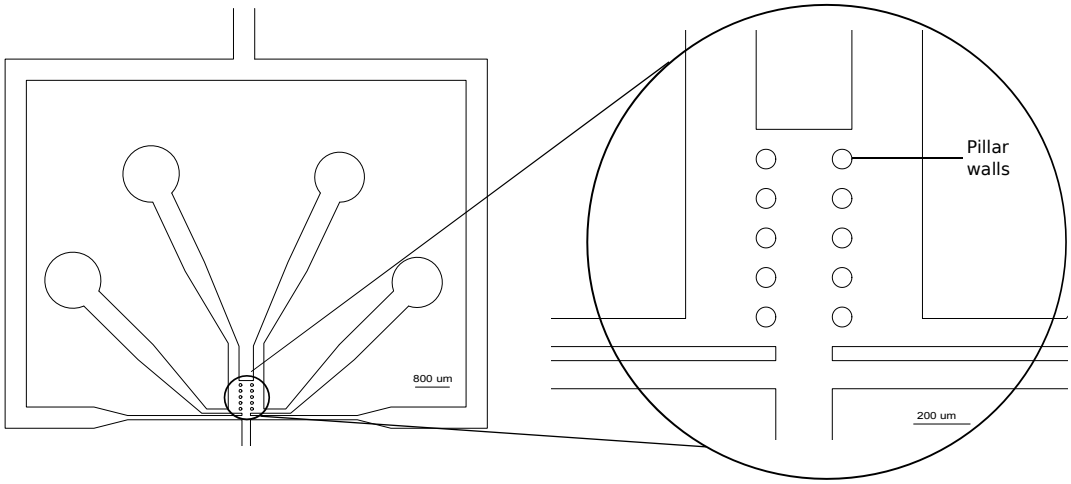

Figure 4.13: Autocad first design with integrated electrodes: On the left side is possible to see the design with integration of solid electrodes and on the right side a zoom of the chamber with pillar walls. More information relative to chip sizes in Appendix B

The initial measurements with buffers were promising. A difference in the impedance value changing with different salt concentration (sodium chloride) buffers was registered, as observed in Figure 4.15. It is also possible to observe the fitting line of the values to equation 4.2.

As referred in Chapter 2 $R = \rho\frac{L}{A}$. R' was added to the equation to estimate the lower

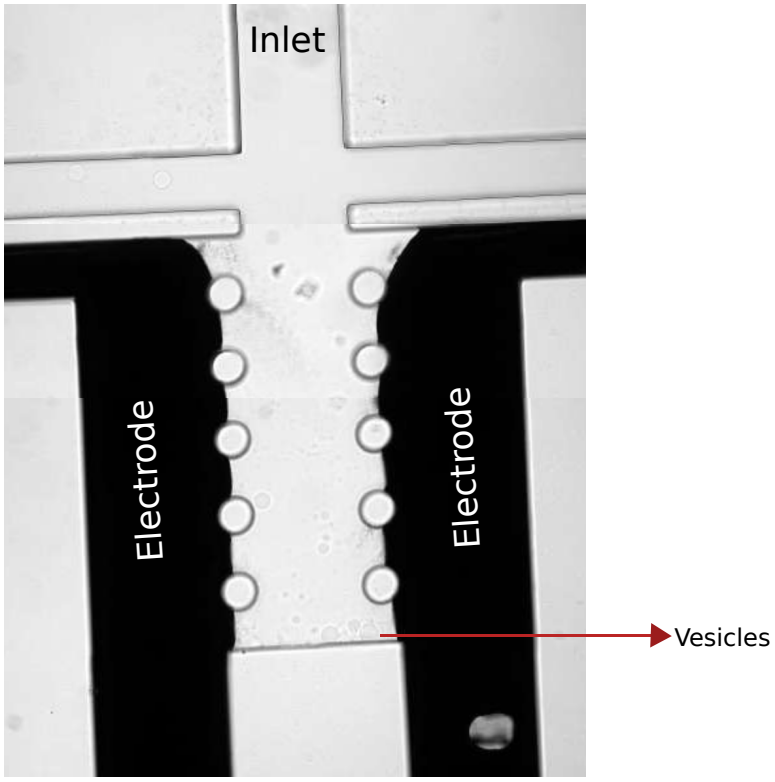

Figure 4.14: Microscope image of the solid electrode walls design.: Some vesicles observed in the bottom of the chamber, image in bright field. Image composed by three separated images with 20x.

resistance the device with geometry can offer to the current. For electrolytes in high concentration $\rho = \frac{1}{\Lambda_{m0}C - K\sqrt[3]{C}}$ in this conditions is possible to estimate values for K that represents the rate of decreasing conductivity at high concentrations and the minimum resistance of the device (R'). using 4.2

$$R = \frac{1}{\Lambda_{m0}C - K\sqrt{C^3}}\frac{L}{A} + R' \tag{4.2}$$

The theoretical values for resistance were also calculated through equation 4.3 and plotted

$$R = \frac{1}{\Lambda_{m0}C}\frac{L}{A} \tag{4.3}$$

Table 4.1: Resistance values: Experimental and theoretical

Salt Concentration	**1 mM**	**10 mM**	**50 mM**	**80 mM**	**100 mM**
Experimental values (kΩ)	137.8	50.6	18.5	10.6	9.7
Calculated values (kΩ)	210.9	21.1	4.2	2.6	2.1

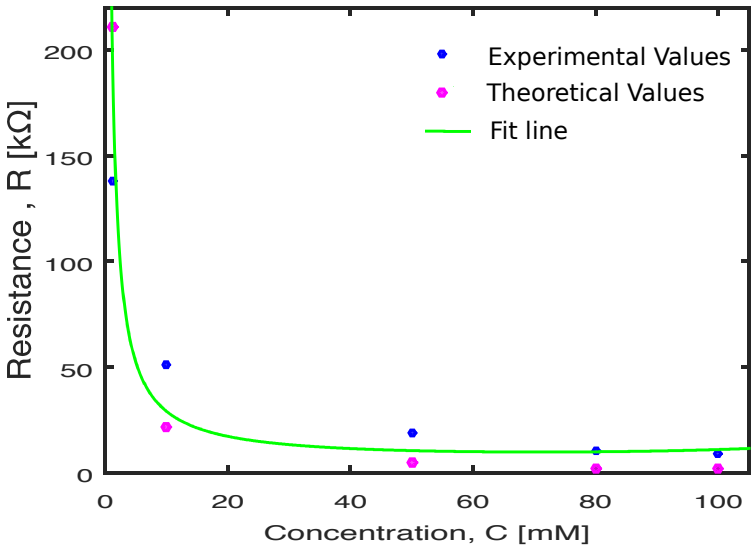

Figure 4.15: Resistance experiment, calculated and fit plots: Values of resistance versus buffer concentration, theoretical values, experimental values and respective fitting line obtained in MATLAB

The experimental and theoretical results are in the same order of magnitude however the values are considerably apart, this might be because of the electrode area considered in the calculation. The technique uses pillars to stop the molten alloy to go in the chamber and so the electrodes surface is slightly domed, this factor of curvature is unknown and it might be possible to have an error that explains the divergence in the values.
For this fitting K was estimated as $3.049X10^{-6}$, the value was not found in the literature, and R' has a value of 9.28 kΩ.
To be able to measure impedance change caused by adhesion is necessary to have a vesicle media packed enough to enable the adhesion to easily happen when the linker is added. Fill the chamber up to the top was the limiting step in this work. GUVs were filled at a 1 part of GUVs to 3 of buffer, which was the dilution with better results in the previous experiments. After microscope observation was possible to assess that the chamber was 1/10 full, so it was flushed again the same diluted suspension, and when the device was imaged again the chamber had less GUVs than before. The device was flushed again and the results did not improve. This might happen because the molten alloy is not homogeneous when suffers the melting and solidifies in the channels, what create sometimes holes in the electrode, which work like pores; and because of the deformable property of the GUVs, they might be being pushed away through those holes. Was tried an improvement of the design with the same configuration but with a smaller chamber. This time the chamber would have 470 μm instead of 750 μm length, width of 100 μm in stead of 200 μm and the pillars spaced by 60 μm, figure 4.16.

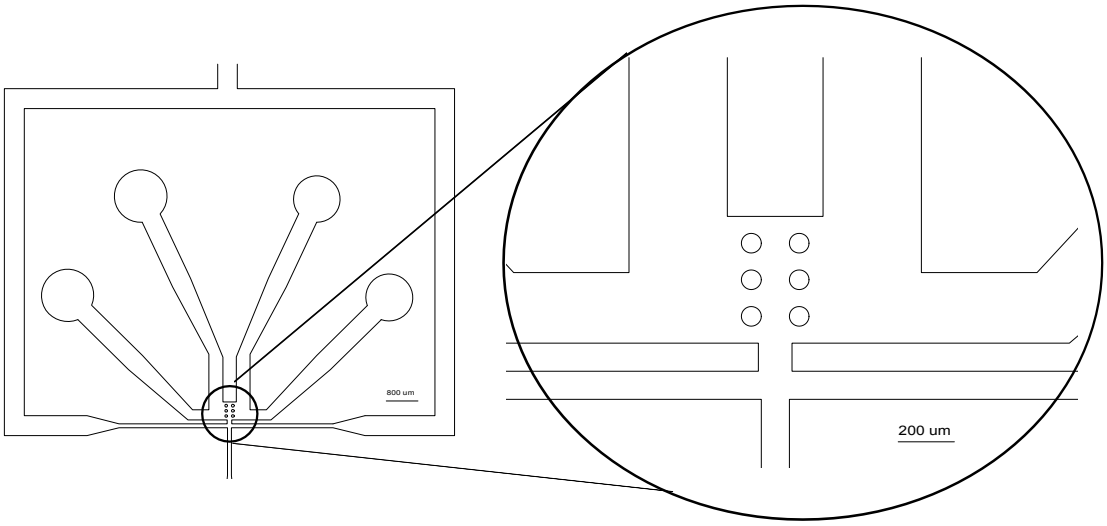

Figure 4.16: Autocad design pillars electrodes with small chamber: Developed from the previous design. On the left side is possible to see the design with integration of solid electrodes and on the right side a zoom of the chamber with pillar walls that separate main chamber from and electrodes channels on the sides,as in the figure 4.13. More information relative to chip sizes in Appendix B

4.2 Design of a biomimetic DNA Adhesion System

In this work the adhesion uses synthetic DNA strands that hybridise at room temperature. Nupack [57] is an online free tool where available to design and analyse DNA systems and where the present system was designed .

The systems was built on four Base anchor strands already designed and optimised to decrease non-desired interactions and with an available single strand to attached the rest of the system that can be changed accordingly to the desired functions. In Figure 4.17 a) represents the anchor strands. These are two anchors of two strands each, that have a double stranded part to build the anchor part and a single stranded part where the rest of the system can be built on, depending on the need. The designing of the system had by base the part to hybridise with the anchors and a 8bp free single stranded that would be complementary to the linker, sequences are in Appendix C. The linker has in total 16bp, 8bp bind to A and 8bp bind to B this way the DNA bridge is created and there is no risk of loop-like conformations as seen in Chapter 1. Also this enables a controlled adhesion, because it will just happen when the linker is added. The anchored strands Bb, B_{bb} and Cb, C_{bb} are annealed with A and B, respectively. These are the construct that functionalized the vesicles.

DOPC vesicles can be functionalized with cholesterol anchored DNA, because of its membrane composition that have cholesterol in it. The strands that functionalized the vesicles were designed not to interact with each other without a presence of the linker. The linker establishes a stable adhesion, the systems is outlined in figure 4.17.

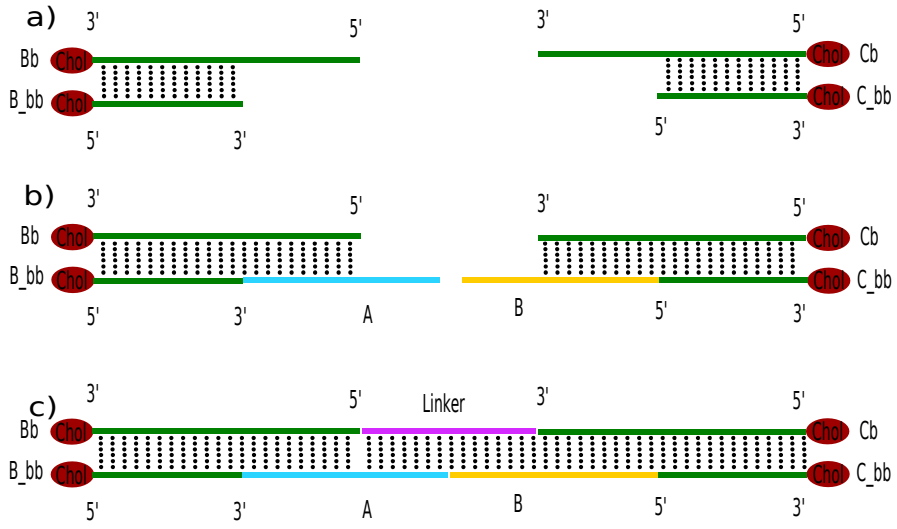

Figure 4.17: DNA system design steps: a) Base system already designed and optimised with two cholesterol anchors that will anchor the DNA strands in the vesicle bi-layer. These strands have 18 hybridised bases and one single strand of 18 bases available on each construct to attach the rest of the system. b) A and B were designed to attach the available strand of 18 bases and have 8 free bases to stick to the linker. A and B for it self don't interact. c) Complete system, Linker is made of 16 bases, it stick 8 to each side (A and B) all together make the final system of adhesion between GUVs.

The system was characterised with two techniques UV-visible and gel electrophoresis. The UV-Vis was carried out on a equipment named Varian Cary 50. The DNA was submitted to a temperature ramp on UV-Visible to find the melting temperature of the different combination of strands. Was made a combination of A + Linker, B + Linker, A + B + Linker, A + B. This because was wanted to study the behaviour of each combination by itself so it was possible to find any anomaly in the system if there is any. This combinations was also used to run the gel electrophoresis. The results for UV-Vis are the following represented in figures 4.18 to 4.25

For this kind of measurements one can find out if the strands are interacting or not, this can be observed in the line of absorbance if the the solution submitted to a ramp of temperature shows a sigmoidal behaviour. This experiment was chosen a ramp of temperature beginning at 15 C°C and ending at 85 °C with a increment of 0.2 °C per min. The absorbance value of a single stranded DNA is higher than a double stranded, so when there is interaction is expected to see a significant change in the absorbance figuring a sigmoidal curve which the middle point is the melting point that give us the respective melting temperature. In the figure 4.18 is possible to see that all of the curves have a slightly slope. It was expected all the samples to have interaction, consequently sigmoidal curve, excepting for A + B sample. This solution is the mixture of the two strands that attach to opposite sides of the bridge and were design to not interact. To have better view

of the behaviour was scaled each curve to suitable range of y (absorbance).

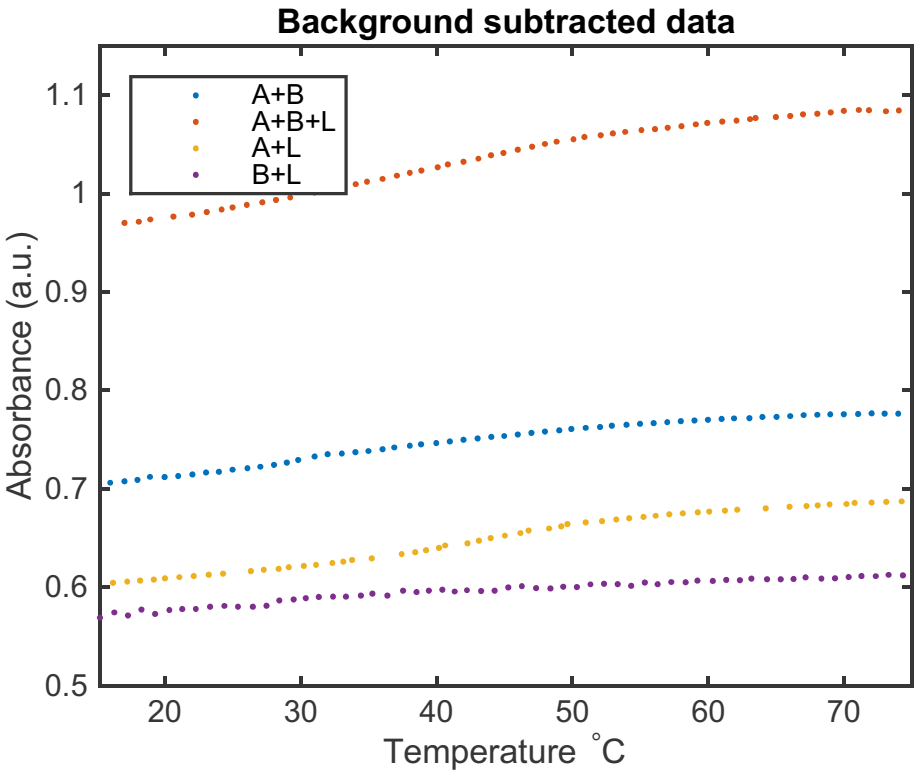

Figure 4.18: UV-Vis curves for all combinations.

In the following figures is showed the experimental results and the simulation of Nupack for respective sample, to compare the expected value of melting temperature of the structures and the experimental one. In figure 4.19, the curve suggests that the interaction expected is happening.The experimental and expected melting points for sample A + Linker are different but very close to each other, being 41.6°C for experimental result and 34.5°C for simulation, as represented on Figure 4.20, A+linker is more stable then expected from the simulation.

In figure 4.21, the curve suggests that the interaction expected is happening, although it has slightly scattered points.The experimental melting point for sample B + Linker is 19.9°C. Regarding the Nupack simulation, in Figure 4.22, the melting temperature simulated is 39,8°C, these values are very different, the system B+Linker seams to be much more stable in the simulation than it actually is.

In figure 4.23, the curve suggests that the interaction expected is happening.The experimental melting point for sample A + B + Linker is 37.3°C. Regarding the Nupack in Figure 4.24 simulation the melting temperature for the simulation is 39,9°C, the melting temperatures are very close and both very satisfactory, because the system is very stable at room temperature.

In figure 4.25, the curve suggests that A and B are slightly interacting, this should not happen because A and B are neither expected or designed to interact. This might

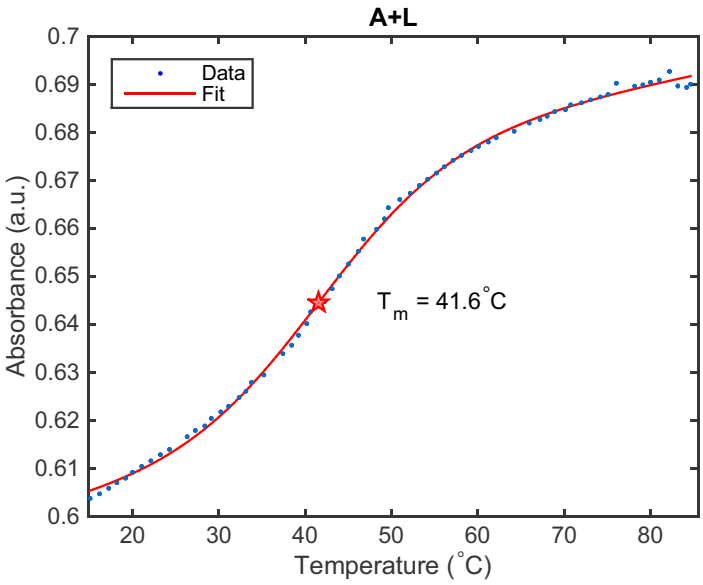

Figure 4.19: UV-Vis curve for A + Linker: Melting point represented in the plot

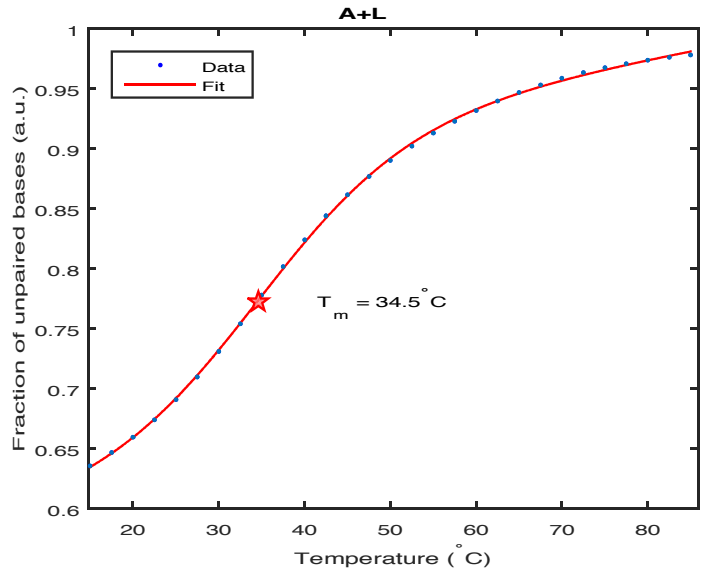

Figure 4.20: Nupack simulation of UV-Vis curve for A + Linker: Melting point represented in the plot

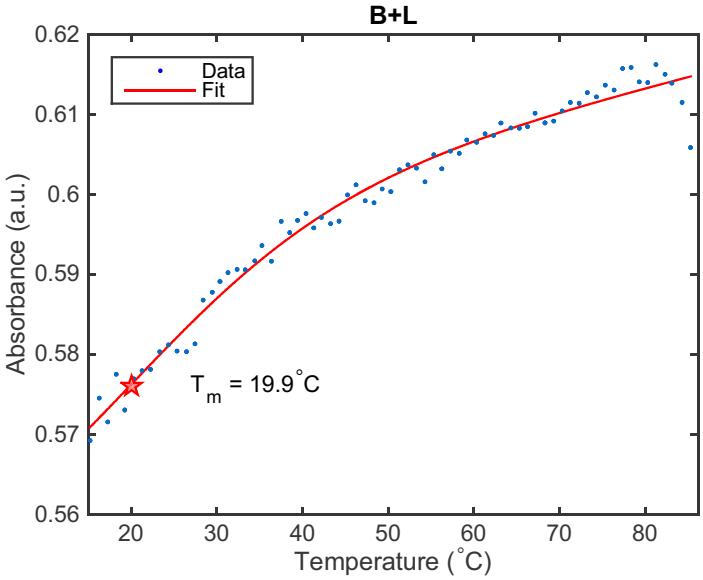

Figure 4.21: UV-Vis curve for B + Linker: Melting point represented in the plot.

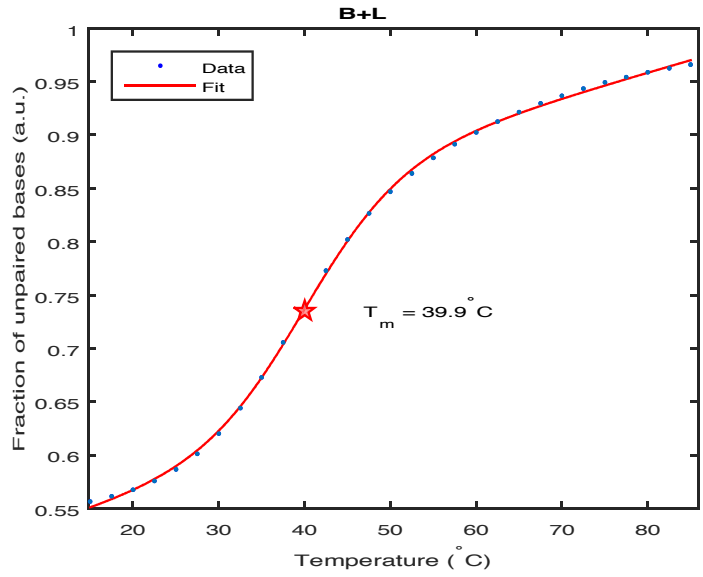

Figure 4.22: Nupack simulation of UV-Vis curve for B + Linker: Melting point represented in the plot.

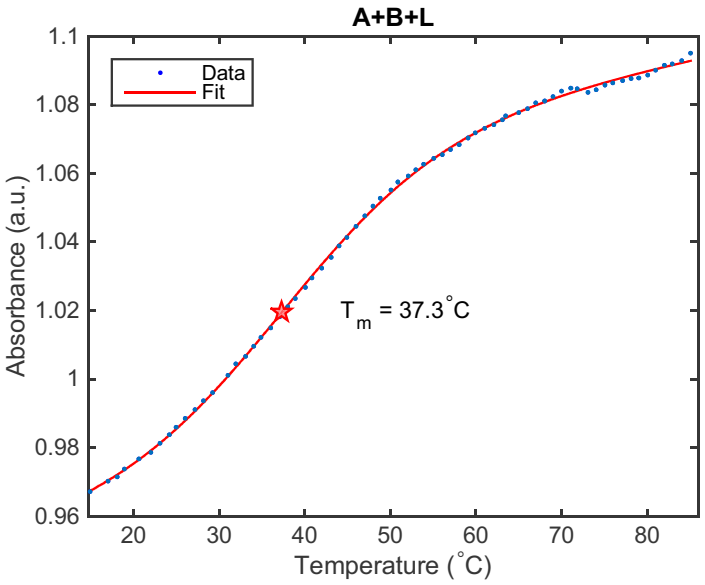

Figure 4.23: UV-Vis curve for A + B + Linker: Melting point represented in the plot

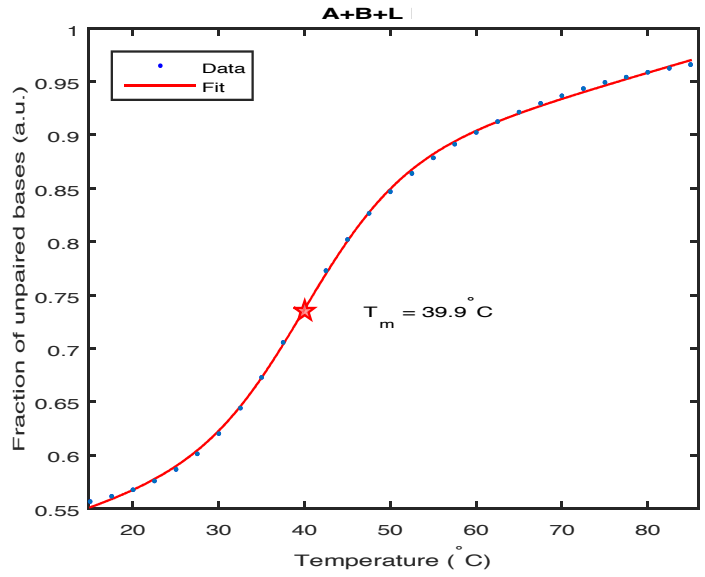

Figure 4.24: Nupack simulation of UV-Vis curve for A + B + Linker: Melting point represented in the plot

be a lack on the system design or because of the anchoring part of the strands A and B are very similar so they can be interacting, although when in the real system they are anchored before being in the same system which means that the only available part to interact is the 8bp design to bind with the linker. Regarding the Nupack simulation A+B has a similar behaviour as in the experimental result.
To go deeper in what is happening in the system was performed an agarose gel electrophoresis but the A and B were annealed with the anchor strands without cholesterol.

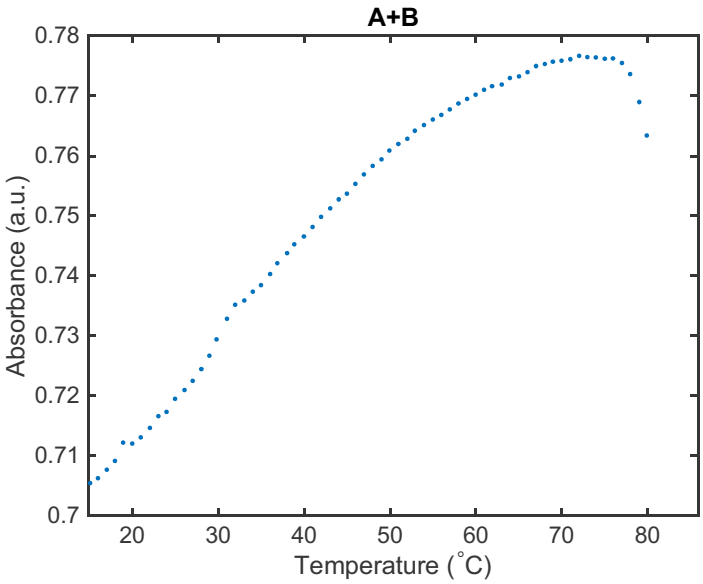

Figure 4.25: UV-Vis curve for A + B

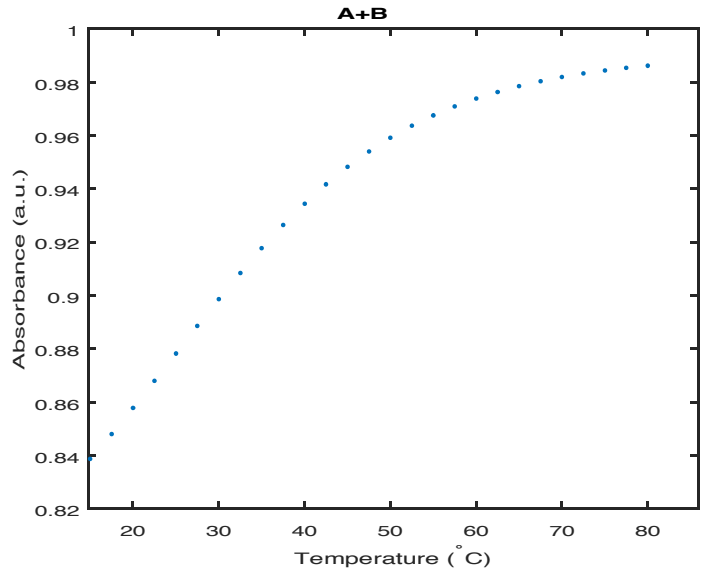

Figure 4.26: Nupack simulation of UV-Vis curve for A + B

In Figure 4.27 is represented the agarose gel electrophoresis results. The gel was run

for 2 hours. Grey value was measured in all bands individually, accordingly to the distance in pixels from the top of the figure. This analysis enables to have a quantitative value for each band. The peak corresponds to the bands' most brighten point, that is assumed to be where the major part of the material is.
The first and last columns are the lader and all other columns are the constructs analysed. The lader is not very well resolved, this maybe because of more time needed running the gel.
A and B are annealed with its respective anchors and are the smallest constructs run. This means that its bands should be the ones on lower position in the gel because they can easily pass through the gel pores, which can be confirmed in the image and also can be analysed in Figure 4.28 and 4.29. The peak values are 751 and 758 in distance and $18.4x10^3$ and $21.5\ x10^3$ in grey value respectively.
A+L and B+L are A with linker and B with linker. They come next in construct size, because of the extra length of the linker and double stranded region between linker an each of the constructs. they expected to have their bands slightly higher than A and B, and both in the same position in the gel. In Figures 4.30 and 4.31 is possible to see the plot referent to A+L and B+L respectively, these peaks have values of distance as 739 in A+B plot and 746 in B+L plot. As expected the values are lower than A and B individually, which means less distance from the top of the figure so higher position compared to the previous ones. Also the grey value is significantly higher being $30.8\ x10^3$ and $27.8x10^3$ for A+L and B+L respectively, this higher value is associated to the extra construct between the linker and A and B separately.
A+B+L is the biggest construct, all bases are paired so the construct is only double stranded DNA which leads to expect higher intensity in the band. The position in the gel is expected to be the highest but in this case it seams to have two bands. The respective plot represented in Figure 4.32 shows two peaks as well. The first corresponds to A+B+L construct at 673 in distance, which is definitely higher than the any other band and the second one to a fraction of A, B and Linker that did not bind all together, this peak appears at 738. This value is very close to A+L peak value which show a better stability for A+L construct than B+L or A+B+L. At the same time the second band is much brighter than the first which means more conformation in A+L or B+L than A+B+L, is possible to calculate the ratio of assembled construct compared with non assembled and is 0.59. The system need to be improved torwards improving A-B-linker structure, to increase the intensity of the band at 673 pixels and decrease the second. The last column in the gel has A and B together to assess if there is interaction between the two as was suspected in UV-vis analysis. This band plot is possible to see in Figure 4.33. The peak for this plot appears at 746 which is the same as B+L this confirms that there is a slightly interaction between these two. UV-vis and this gel were performed with different samples, in the UV-vis the samples A and B were single stranded as they come form the manufacturer but to run the gel the anchor was annealed to A and B to discard the possibility of interaction between the anchor bits of the strands. This because in the real system A and B will never

be without the anchor. The if there was enough time the following step would be to run a gel with A and B single stranded, separately, together and with the linker and A and B anchored as in this gel to compare the results and take due conclusions.
From this gel is concluded that the system needs to be improved because the binding between the three is not as favourable as it is suppose to be. In the final system is very important to have a stable binding between the three because it will mediate the adhesion and no interaction between A and B because this will cause changes in the impedance values before the linker addition and also decrease the sensitivity of the system.

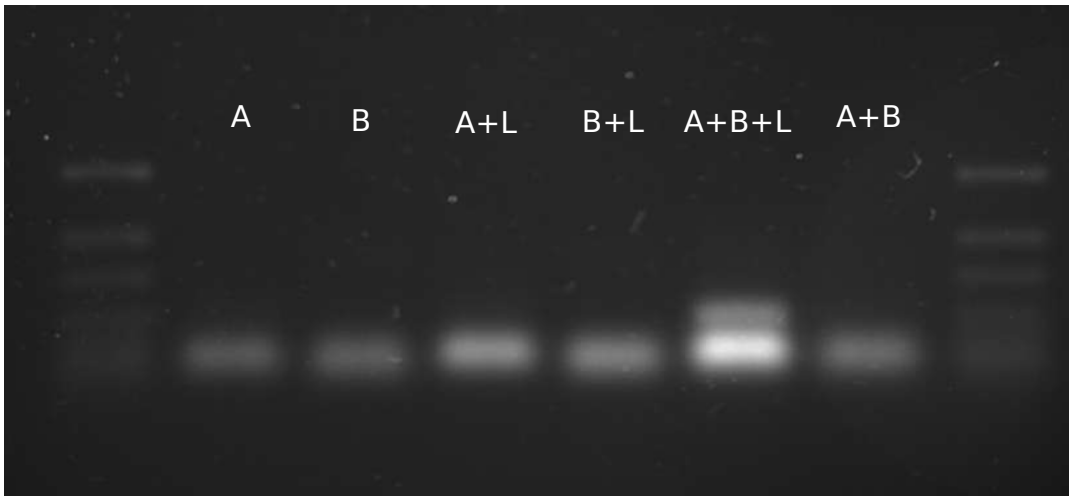

Figure 4.27: Agarose gel electrophoresis: Six samples were run with different combination of A, B and linker as indicated in the figure. A and B are annealed with the anchor strands without cholesterol. (Poor quality of printed version of the image, laders only possible to see in PDF version.)

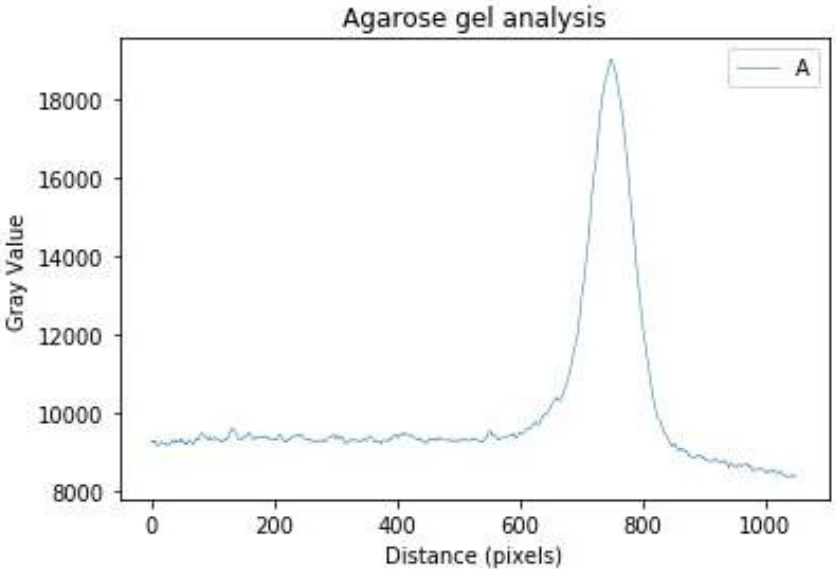

Figure 4.28: Intensity profile of sample A: First column profile grey value as function of distance from the top of the image. Peak values are x=751,y=184049

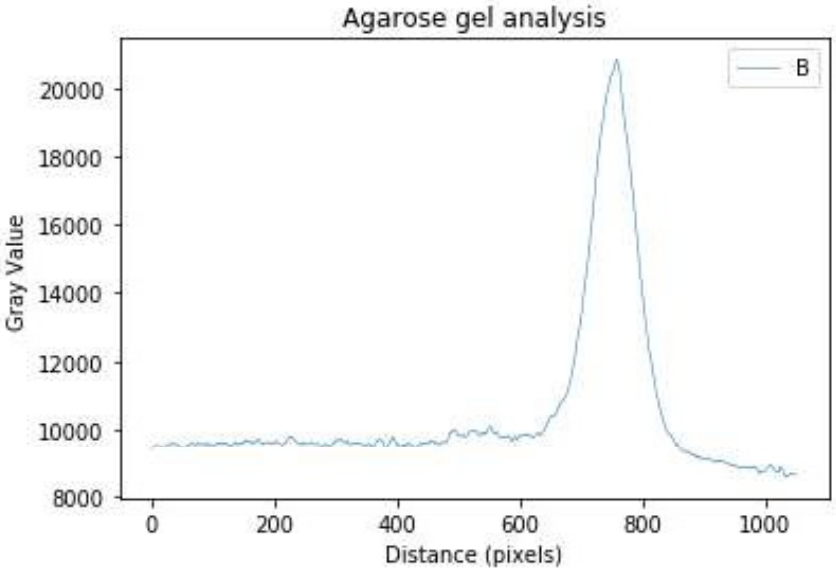

Figure 4.29: Intensity profile of sample B: Second column profile of grey value as function of distance from the top of the image. Peak values are x=758,y=21499

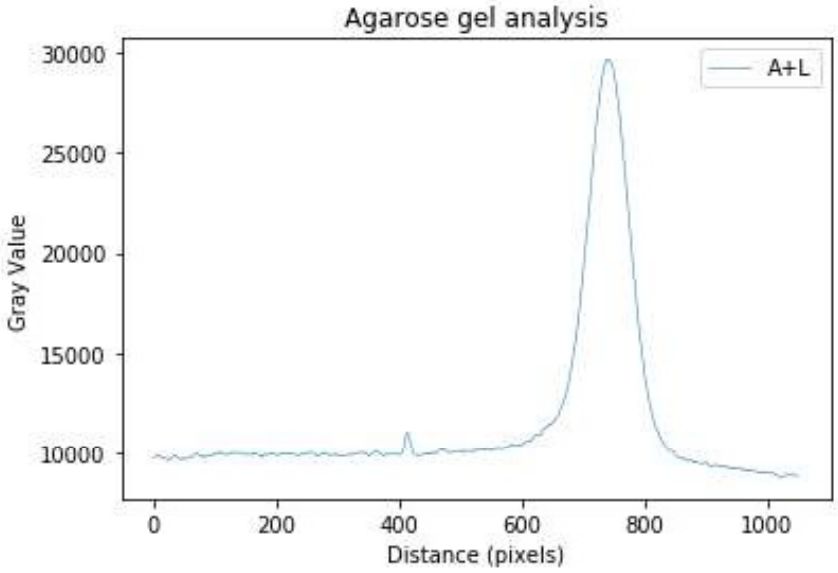

Figure 4.30: Intensity profile of sample A and linker: Third column profile of grey colour of the third column, correspondent to sample A and linker, as function of distance from the top of the image. Peak values are x=739,y=30816

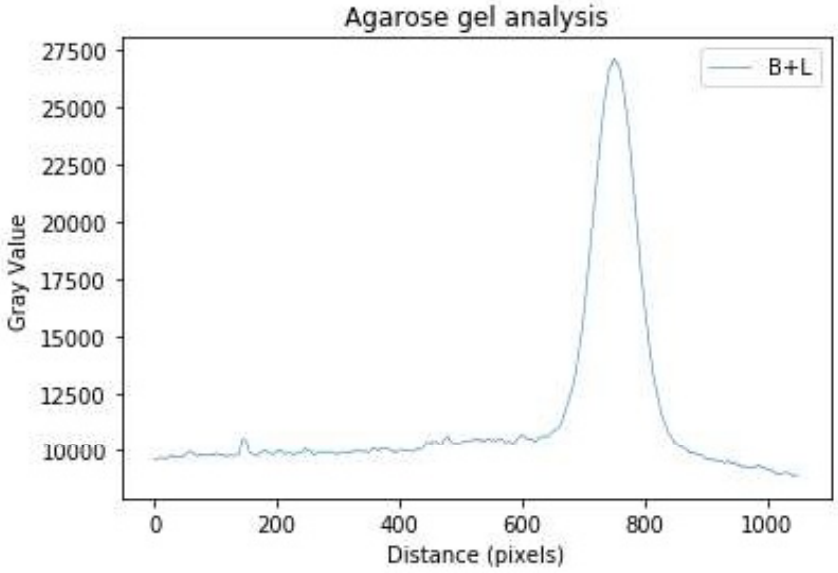

Figure 4.31: Intensity profile of sample B and linker: Forth column profile of grey colour of the forth column, correspondent to sample B and linker, as function of distance from the top of the image. Peak values are x=746,y=27857

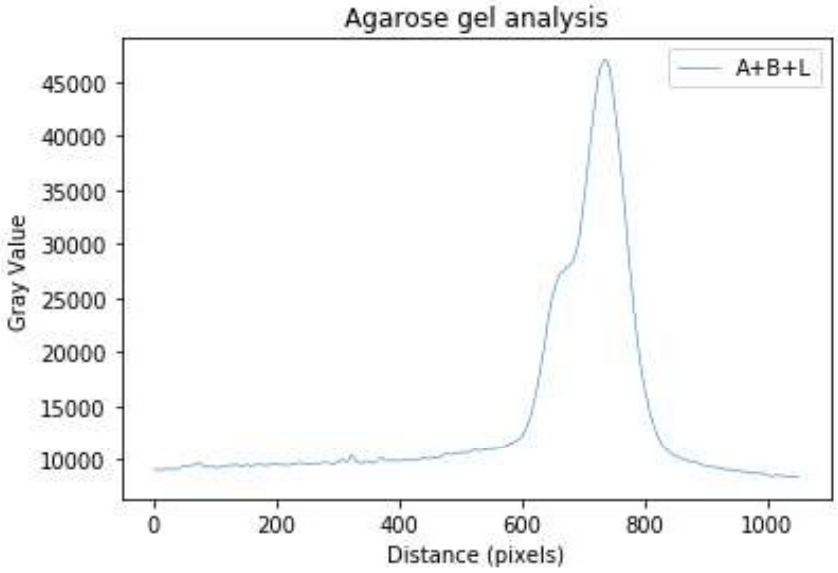

Figure 4.32: Intensity profile of sample A, B and linker: Fifth column profile of the grey colour of the fifth column, correspondent to sample A, B and linker, as function of distance from the top of the image. Peak values are x=673,y=28992

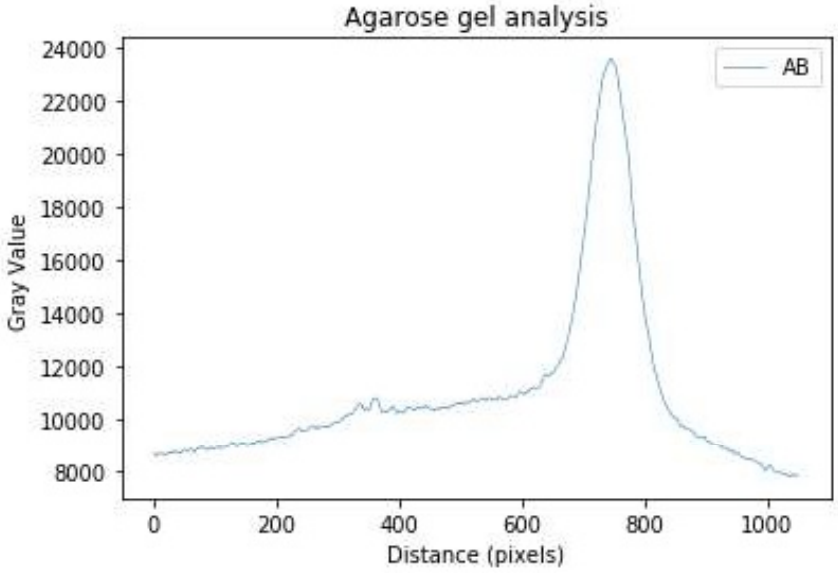

Figure 4.33: Intensity profile of sample A and B: Sixth column profile of the grey colour of the sixth column, correspondent to sample A with B, as function of distance from the top of the image. Peak values are x=746,y=24293

4.3 Impedance Measurements

The final impedance measurements were made to a GUVs suspension with and without linker and was tried to identify the change in the impedance. As referred before in section 4.1 because of the electrodes are in contact with solution impedance is measured as resistance. In the Figures 4.34 to 4.41 the GUVs suspension is already functionalized, there is no linker in the device. They were flushed and the devices were in upwards position for 1h and then flushed again and it was waited for another hour in upwards position. A single value was registered to have a reference state of the resistance of the media, in Figures 4.34 to 4.36 the resistance measured in the media is 18.78 kΩ. For Figures 4.39 to 4.41 the single impedance value is 38.4 kΩ. Figures 4.38 and 4.39 are the bright field images of Figures 4.35 to 4.36. In this images is possible to observe the chamber of two devices. The black side areas are the electrodes, the round shapes are the pillars and the bright material are vesicles. In the lipid mixture is added texas-Red that is a fluorescent dye. This enable to have a better look on GUVs on the microscope since the contrast between the GUVs and the background is no always ideal and more important than that is that is by measuring the brightness intensity that is possible to affirm that the adhesion is actually happening because when this happens the brightness has double the intensity. It was expected to observe bright vesicles accomulation. in the bottom of the chamber. As is possible to see and as was already referred the electrodes are not homogeneous which can cause holes where the GUVs can go through as is Figure 4.36. Also is possible to see that the alloy does not wet the walls that cause a narrow gap all along the walls, this is the main reason for the GUVs not stay in the chamber, because there is actually a little flow that goes through the electrodes and they are pushed away. New experiments focused on low flow-rates are being prepared to improve the chamber filling and enable to measure the impedance of linked vesicles.

There is always a contribution of capacitance and resistance in these measurements so to measure a single value for impedance first is pre-analysed two graphics that represent the impedance values in a range of frequencies and a phase graphic that shows the phase of that measurement. The phase graphic gives the better frequency to take the impedance value. For resistance phase equals to zero, and the frequency in the phase graphic that represents phase zero is the one that will be used to take the single measurement.
To be able to test if in fact the vesicles adhesion would influence the impedance measurements that to prove that the work around the chip is worth, was tried to make a simple measurement in an observation well, that is possible to see in Figure 4.42. The wires of the alloy were placed in the sides of the well and sticked with conductive tape, as showed in Figure 4.43 and the connection was made in the same way with the same equipment and in the microscope at the same time, Figures 4.44 and A.1.

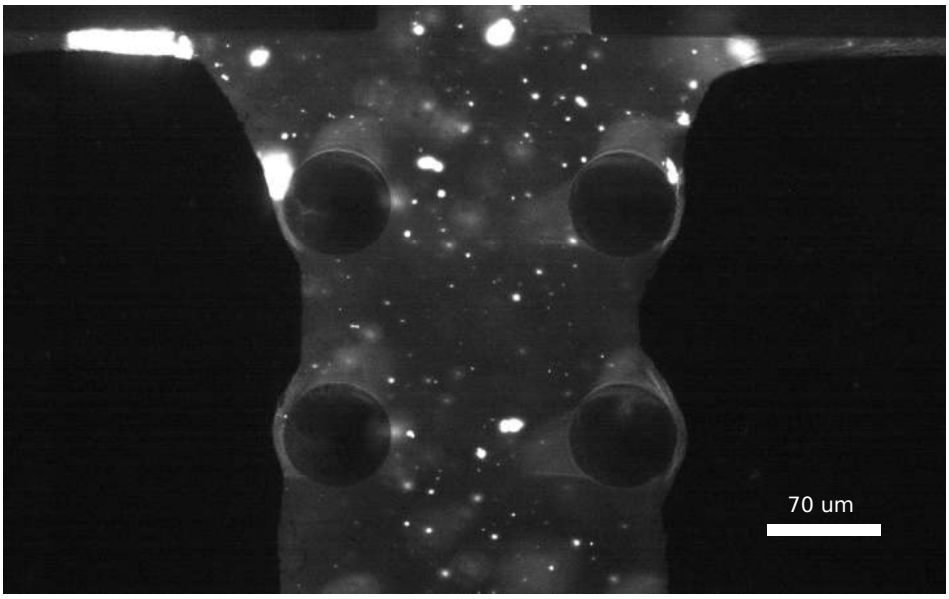

Figure 4.34: Microscope image of microfluidic device in fluorescence with 40x objective. Top of the chamber

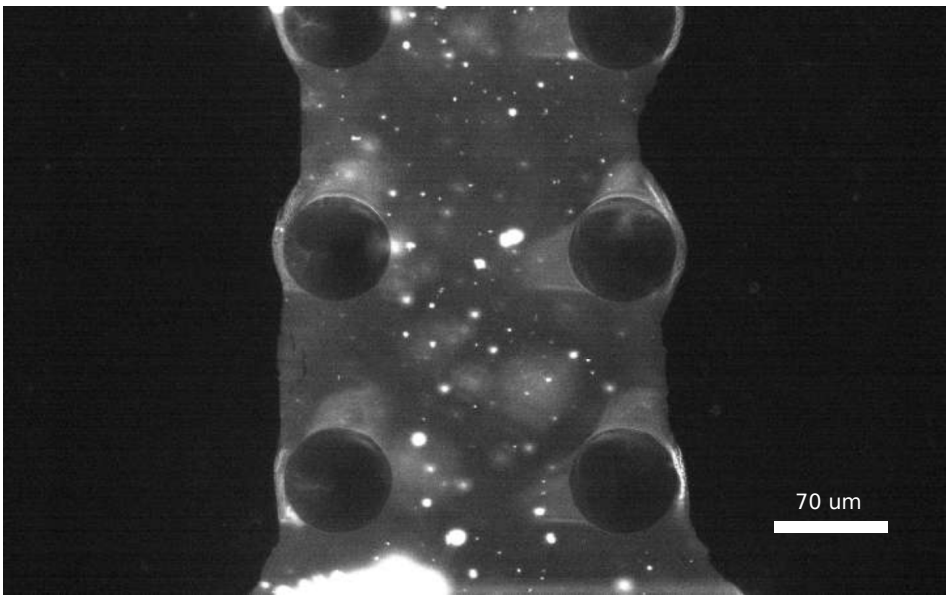

Figure 4.35: Microscope image of microfluidic device in fluorescence with 40x objective. Middle of the chamber

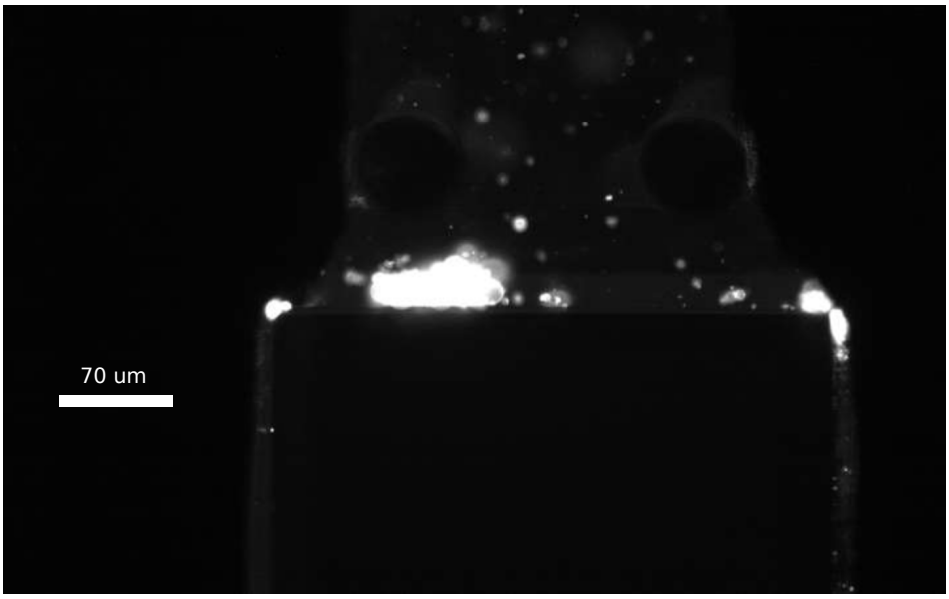

Figure 4.36: Microscope image of microfluidic device in fluorescence with 40x objective. bottom of the chamber

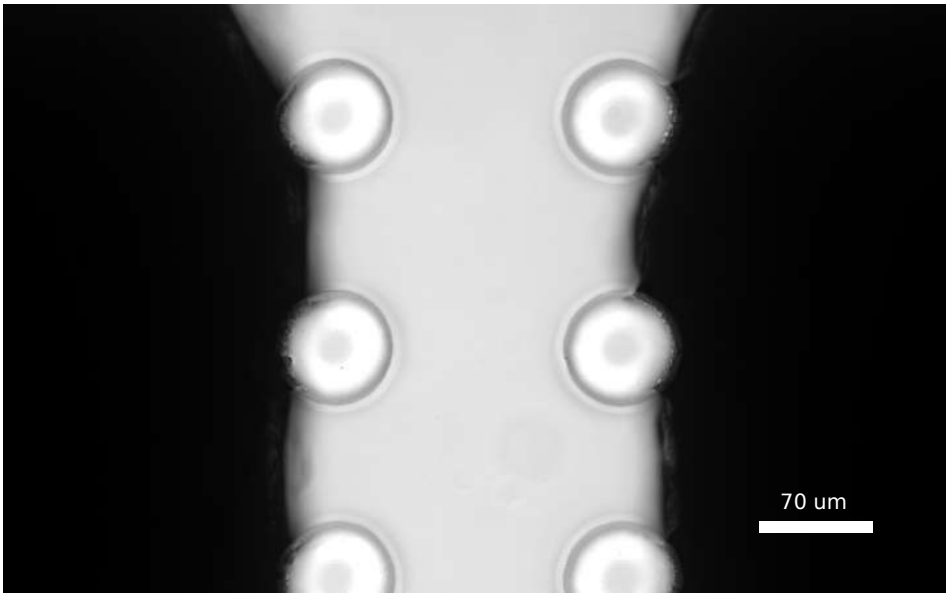

Figure 4.37: Microscope image of microfluidic device in bright field with 40x objective. Middle of the chamber

Figure 4.38: Microscope image of microfluidic device in bright field with 40x objective: Bottom of the chamber. Is also possible to see the vesicles in the bottom, matching the fluorescence image.

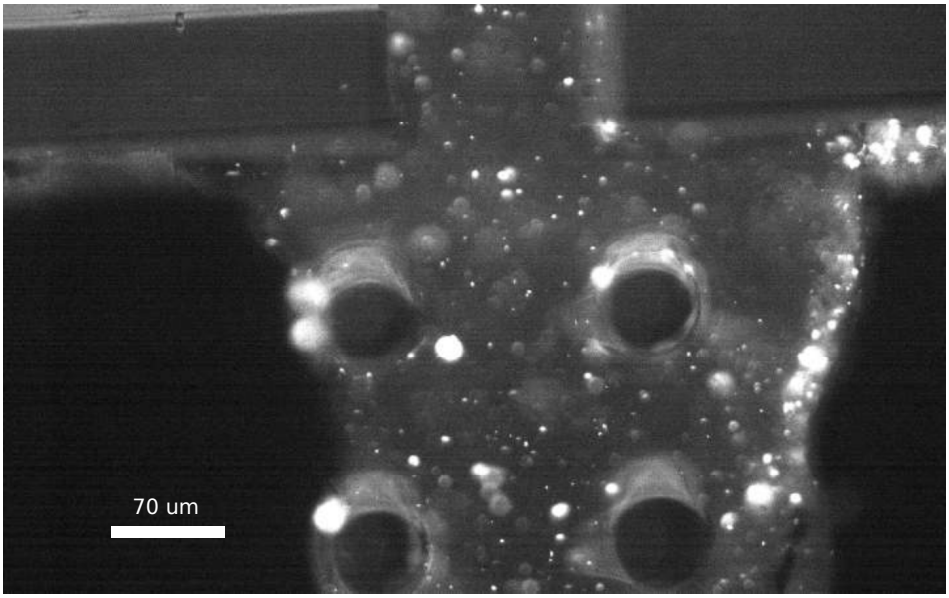

Figure 4.39: Microscope image of microfluidic device in fluorescence with 40x objective. top of the chamber

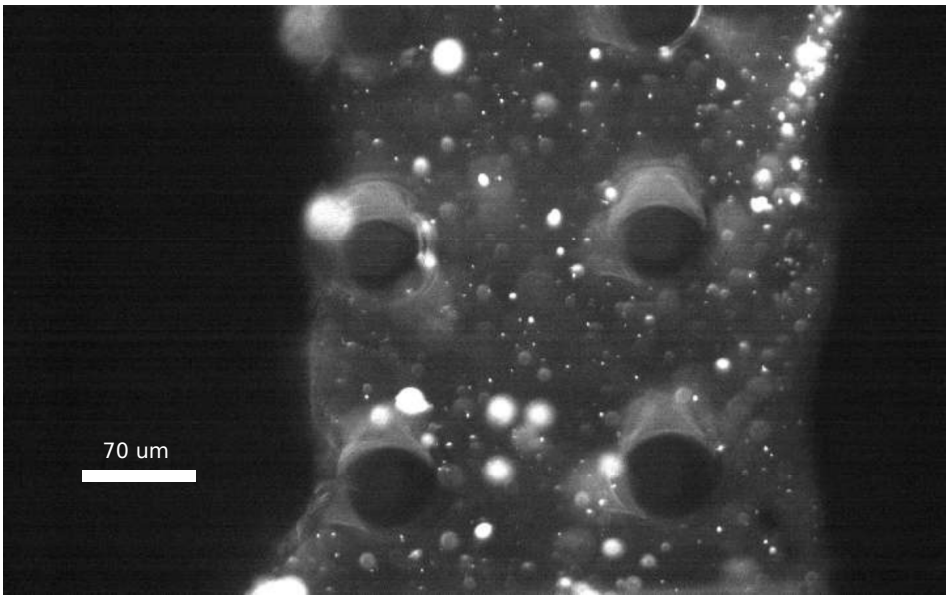

Figure 4.40: Microscope image of microfluidic device in fluorescence with 40x objective. middle of the chamber

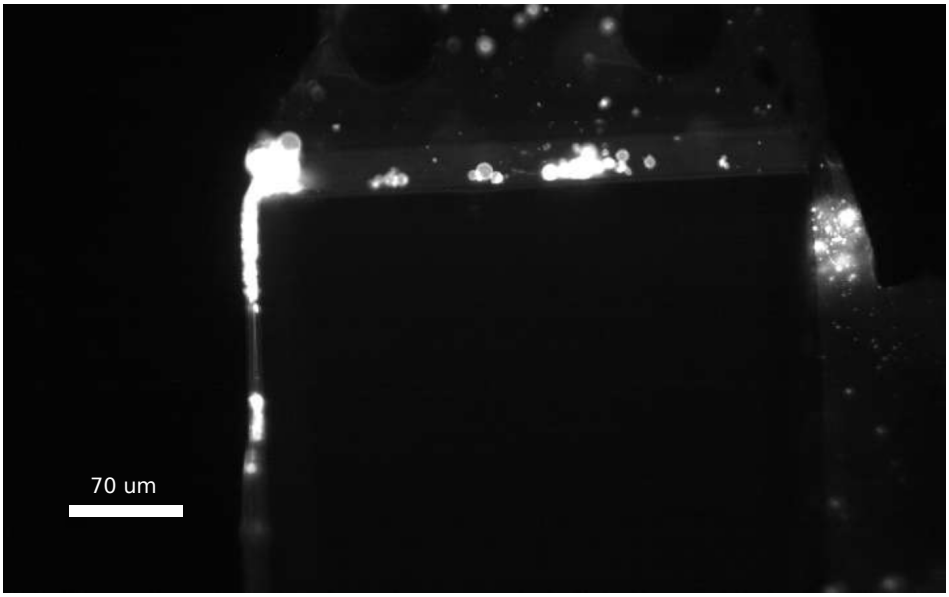

Figure 4.41: Microscope image of microfluidic device in fluorescence with 40x objective: Bottom of the chamber. Is possible to see the GUVs escaping through the electrodes gaps.

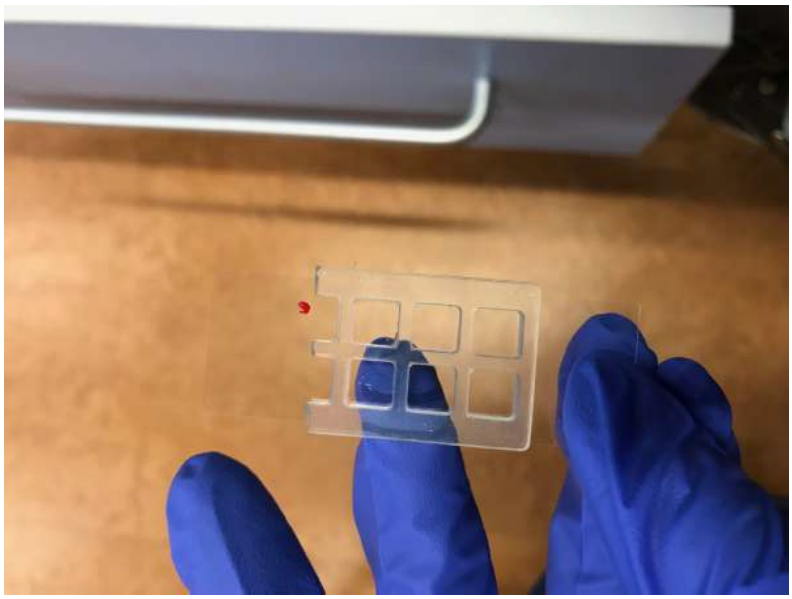

Figure 4.42: Observation well

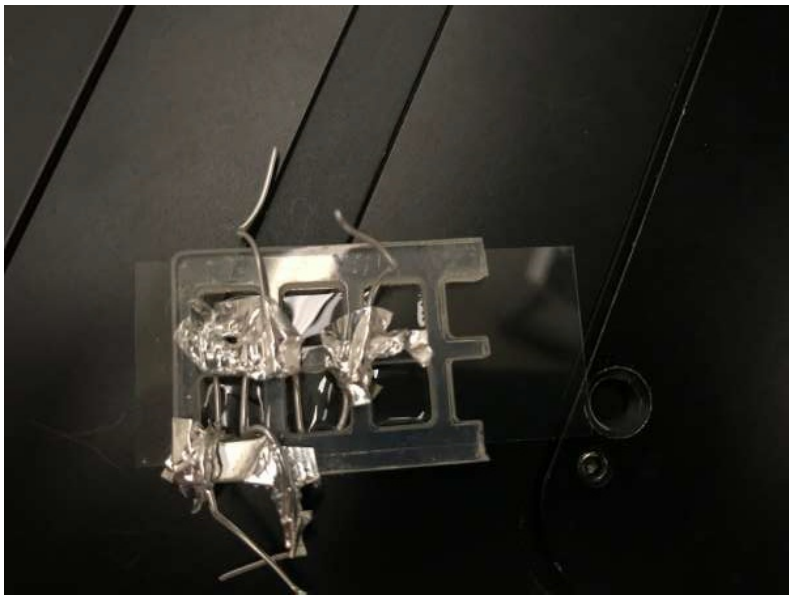

Figure 4.43: Observation well assembled to measure impedance: Electrodes are the wires of the Indium alloy on the sides of the well

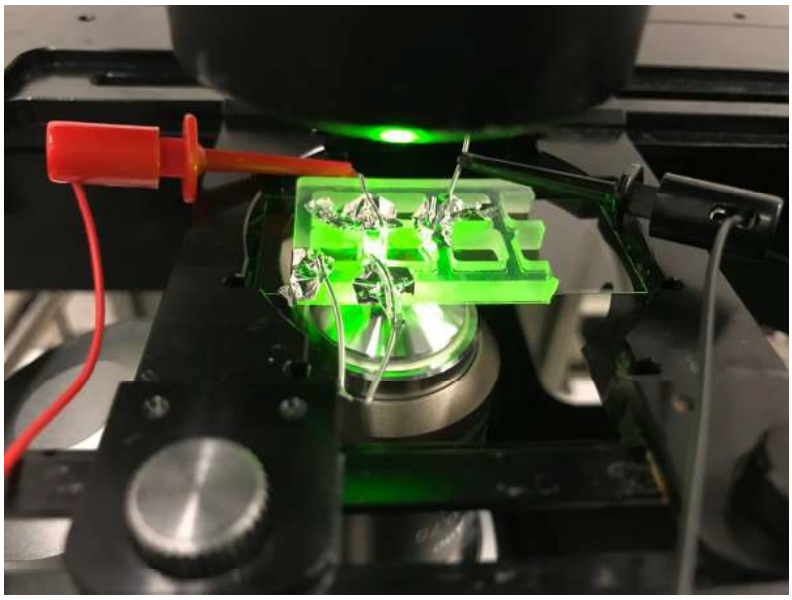

Figure 4.44: Observation well in the microscope: Exposed to fluorescence light connected to measurement equipment.

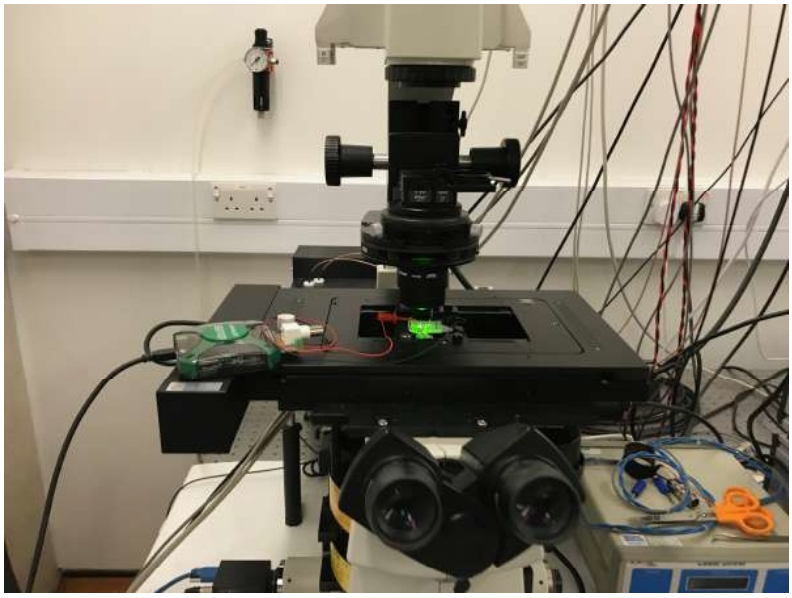

Figure 4.45: Set-up used to make the impedance measurements with observation well.

The suspension placed in the well was the same flushed in the devices previously, 50μL of functionalized GUVs at 0.7μM. The linker was added after the first measurement. A value of 1.147kΩ was registered for this stage at 100 kHz. A 50μL volume of Linker was added in the well at a concentration of 2μM, to match the constructs concentration. After the linker addition, which caused movement in the sample the GUVs start moving and adhering. The resistance value increased to a value of 2.114kΩ ate 100kHz. To understand where this change comes from is necessary to reproduce this measurement at least three times in the same conditions and also other experiments to see if in fact it comes from the adhesion.

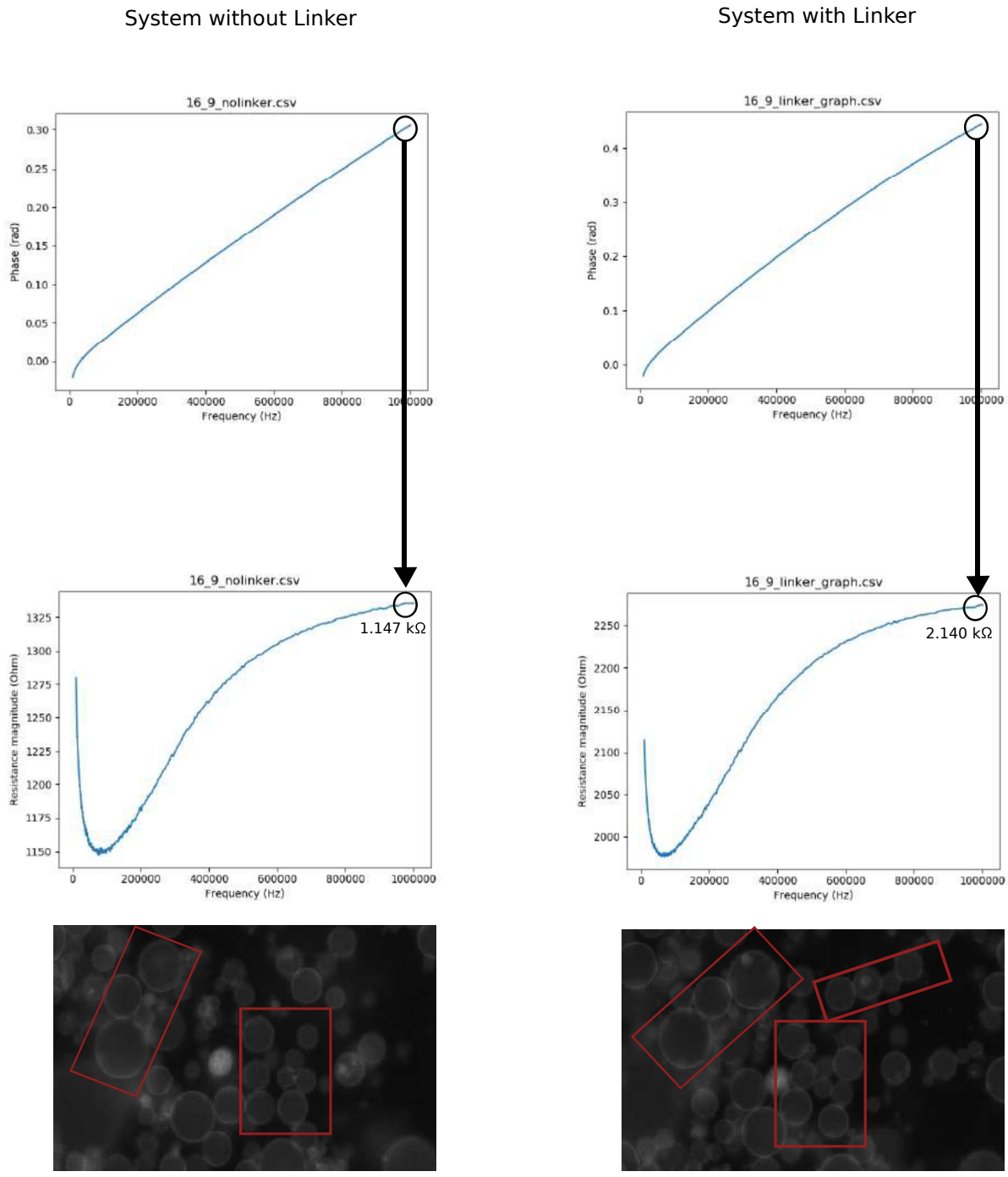

Figure 4.46: Impedance measurement results in observation well: The phase plot enables to chose the best frequency to take a single measurement. At 100 kHz, frequency chosen to take the measurement, was registered the respective indicated value in both conditions.

Chapter 5

Conclusion and future work

A microfluidic platform was designed and improved resulting in a device where is possible to perform impedance measurements. This design needs further improvement to enable fine and easy control of the vesicles diffusion and easy filling of the chamber with vesicles to perform the impedance measurements in a controlled flow-less system.
Filling the device was one of the big challenges in this work. It is very hard to control vesicles in such small features and there is a point of improvement that will help a lot this system to work better and develop faster.
A DNA system was successfully designed and characterised as shown in Chapter 5. It can still be improved to have better sensitivity and to decrease noise in the measurements caused by undesired interactions between the structures. This can be done by decreasing similarity between A and B or also by increasing the length of A and B linker-sticky-end because this will stabilise the interactions between A and linker, and B and linker respectively and again prevent non-desired interactions.
The final measurements showed a change in the impedance when the linker was added and that is attributed to adhesion between vesicles, but further experiments need to be done at this stage. These results still need to be reproduced and probe appropriate controls that confirm that vesicle adhesion and aggregation are responsible for the changes detected in impedance measurements.
This work opens a possibility of varying the parameters and find other ways to sense analytes with DNA using impedance measurements and DNA aptamers.
The next step is to perform the impedance measurements of the adhesion in the device chamber.
Further work can be done based on this proof-of-concepts such as opening the applications range of the device to other analytes.

Bibliography

[1] N. Bhalla. "Introduction to biosensors." In: *Essays in Biochemistry* 10 (2016). ISSN: 0362-1340. DOI: 10.1042/EBC20150001.

[2] M. Chakraborty. "An Overview of Biosensors and Devices." In: *Elsvier* 10 (2017). DOI: 10.1016/B978-0-12-803581-8.10316-9.

[3] P. Mehrotra. "Biosensors and their applications – A review." In: *Elsvier* 10 (2015). DOI: 10.1016/j.jobcr.2015.12.002.

[4] J. Dinic. "The T cell receptor resides in ordered plasma membrane nanodomains that aggregate upon patching of the receptor." In: *Scientific Reports* 5 (2015). DOI: 10.1038/srep10082.

[5] D. Bax. "Fundamental insight into the effect of carbodiimide crosslinking on cellular recognition of collagen-based scaffolds." In: *Acta Biomaterialia* 49 (2017), pp. 218–234. DOI: doi.org/10.1016/j.actbio.2016.11.059.

[6] L. Parolini. "Volume and porosity thermal regulation in lipid mesophases by coupling mobile ligands to soft membranes." In: *Nature Comunications* 10 (2014). DOI: 10.1038/ncomms6948.

[7] J. Steinkühler. "Modulating Vesicle Adhesion by Electric Fields." In: *Biophysical journal* 111 (7 2016), pp. 1454–1464.

[8] O. amjad. "Membrane Adhesion through Bridging by Multimeric Ligands." In: *Langmuir* 33 (5 2017), 1139–1146.

[9] W. Hughes. "The potential difference between glass and electrolytes in contact with the glass." In: *Journal of the American Chemical Society* 44 (1922), pp. 2860–2867.

[10] W. R. Heineman. "Obituary." In: *Science Direct* 21 (2006), 1403–1404. DOI: 10.1016/j.bios.2005.12.005..

[11] A. Turner. "Biosensors: sense and sensibility." In: *Chem. Society reviews* 42 (2013), 3175–3648. DOI: 10.1016/j.bios.2005.12.005..

[12] C. Chen. "Recent advances in electrochemical glucose biosensors: a review." In: *RSC Advances* (14 2013). DOI: 10.1039/c2ra22351a.

[13] Y. Fu and J. Guo. "Blood Cholesterol Monitoring With Smartphone as Miniaturized Electrochemical Analyzer for Cardiovascular Disease Prevention." In: *IEEE Trans. Biomed. Circuits Syst* 12 (2018), 784–790.

[14] J. Guo. "Smartphone-Powered Electrochemical Dongle for Point-of-Care Monitoring of Blood -Ketone." In: *Anal. Chem* 89 (2017). DOI: https://doi.org/10.1021/acs.analchem.7b02531.

[15] X. H. et al. "Smartphone-Based Blood Lipid Data Acquisition for Cardiovascular Disease Management in Internet of Medical Things." In: *IEEE Access* 7 (2019).

[16] T. Bhardwaj. "Review on Biosensors Technologies." In: *International journal of advanced researsh in engeneering and technology* 6 (2 2015), 36–62. ISSN: 0976 - 6499.

[17] J. S. J. Cabaj. "Electrochemical Nanosized Biosensors: Perspectives and Future of Biocatalysts." In: *Journal of Analytical Bioanalytical Techniques* (2013). DOI: 10.4172/2155-9872.S7-005.

[18] J. K. P. Damborský J. Švitel. "Electrochemical Nanosized Biosensors: Perspectives and Future of Biocatalysts." In: *Essays in biochem* 60 (2016), 91–100. DOI: 10.1042/EBC20150010..

[19] M. Pohanka. "Overview of Piezoelectric Biosensors, Immunosensors and DNA Sensors and Their Applications." In: *Materials* 11 (2018). DOI: 10.3390/ma11030448.

[20] B. Xie and B. Danielsson. "Thermal Biosensor and Microbiosensor Techniques." In: *Wiley online Library* (2008). DOI: https://doi.org/10.1002/9780470061565.hbb065.

[21] Z. Q. Guan JG Miao YQ. "Impedimetric Biosensors." In: *Journal of Bioscience and Bioengineering* 97 (4 2004), 219–226. DOI: 10.1016/S1389-1723(04)70195-4.

[22] R. F. A. Sauma. "Use of substrate coated electrodes and AC impedance spectroscopy for the detection of enzyme activity." In: *Biosensors Bioelectronics* 13 (1998), 511–518.

[23] R. Naumann. "The peptide-tethered lipid membrane as a biomimetic system to incorporate cytochrome c oxidase in a functionally active form." In: *Biosensors Bioelectronics* 14 (1999), 651–662. DOI: https://doi.org/10.1016/S0956-5663(99)00036-6.

[24] L. Hou. "Graphene oxide-labeled sandwich-type impedimetric immunoassay with sensitive enhancement based on enzymatic 4-chloro-1-naphthol oxidation." In: *Biosensors Bioelectronics* 47 (2013), 149–156. DOI: https://doi.org/10.1016/j.bios.2013.02.035.

[25] R. Elshafey. "Label-free impedimetric immunosensor for ultrasensitive detection of cancer markerMurine double minute 2 in brain tissue." In: *Biosensors Bioelectronics* 39 (2013), 220–225. DOI: https://doi.org/10.1016/j.bios.2012.07.049.

[26] M. Canbaz. "Electrochemical biosensor based on self-assembled monolayers modified with gold nanoparticles for detection of HER-3." In: *Analytica Chimica Acta* 814 (2014), 31–38. DOI: https://doi.org/10.1016/j.aca.2014.01.041.

[27] L. Hou. "DNAzyme-functionalized gold–palladium hybrid nanostructures for triple signal amplification of impedimetric immunosensor." In: *Biosensors Bioelectronics* 54 (2014), 365–371. DOI: https://doi.org/10.1016/j.bios.2013.11.014.

[28] L. M. L. Kubota. "Review of the use of biosensors as analytical tools in the food and drink industries." In: *Food chem* 77 (2002), 237–256.

[29] S. T. Lakshmipriya. "An Introduction to Biosensors and Biomolecules." In: *Nanobiosensors for Biomolecular Targeting* 77 (2019), 1–21. DOI: https://doi.org/10.1016/B978-0-12-813900-4.00001-4.

[30] M. S.E. R. Monošíka. "Biosensors — classification, characterization and new trends." In: *Acta Chem* 5 (2012), 109–120.

[31] R. K. "Recent Advances and Applications of Biosensors in Novel Technology." In: *Biosensors Journal* (2017). DOI: 10.4172/2090-4967.1000145.

[32] B. L.A. T. Chris Calladine Horace Drew. *Understanding DNA*. 3rd. Elsevier Academic Press, 2006. ISBN: 0-12-155089-3.

[33] C. Ashworth. "DNA nanotechnology: Building big with DNA bricks." In: *Nature Reviews Materials* 3 (2018), p. 17092. DOI: 10.4172/2090-4967.1000145.

[34] K. P.V.A. Z. Matthew L. Bochman. "DNA secondary structures: stability and function of Gquadruplex structures." In: *Nature Reviews Genetics* 13 (2012), 770–780.

[35] J. SantaLucia. "A unified view of polymer, dumbbell, and oligonucleotide DNA nearest-neighbor thermodynamics." In: *Proceedings of the National Academy of Sciences* 95 (1998), 1460 – 1465. DOI: 10.1039/c81c01275j.

[36] D. Y. Zhang and G. Seelig. "Dynamic DNA nanotechnology using strand-displacement reactions." In: *Nature Chemistry* 3 (2011), p. 103.

[37] N. C.S.H. F. Sleiman. "DNA nanotechnology." In: *Nature reviews* 3 (2017). DOI: 10.1038/natrevmats.2017.68.

[38] Y. L.H. Y. J. Nangreave D. Han. "DNA origami: a history and current perspective." In: *Current Opinion in Chemical Biology* 14 (5 2010), 608–615. DOI: 10.1038/natrevmats.2017.68.

[39] P. Wang. "The Beauty and Utility of DNA Origami." In: *Chems* 2 (3 2017), 359 – 382. DOI: https://doi.org/10.1016/j.chempr.2017.02.009.

[40] A. H.-J. T. Liedl. "From DNA Tiles to Functional DNA Materials." In: *Trends in Chemestry* (2019). DOI: https://doi.org/10.1016/j.trechm.2019.07.006.

[41] P. Rothemund. "Folding DNA to create nanoscale shapes and patterns." In: *Nature* 440 (2006), 297–302.

[42] K. Abnous. "A novel electrochemical aptasensor forultrasensitive detection of fluoroquinol ones based on single-stranded DNA-binding protein." In: *Sensors and Actuators B Chem* 240 (2017), 100–106. DOI: 10.1016/j.snb.2016.08.100.

[43] M. Danesh. "A novel electrochemical aptasensor based on arch-shape structure of aptamer-complimentary strand conjugate and exonuclease I for sensitive detection of streptomycin." In: *Biosensors and Bioelectronics* 75 (2016), 123–128.

[44] D. Chen. "Development of an aptasensor for electrochemical detection oftetracycline." In: *Food control* 42 (2014), 109–115.

[45] T. H.M. T. T. Azuma Y. Teramura. "Enhancement of Cell Adhesion on a Phosphorylcholine-Based Surface through the Interaction with DNA Mediated by Ca2+ Ionse." In: *Journal of physical chemestry* (2016). DOI: https://doi.org/10.1021/acs.jpcb.6b08741..

[46] K. M.A.S. A. Daraee H Etemadi A. "Application of liposomes in medicine and drug delivery." In: *Artificial Cells, Nanomedicine, and Biotechnology* 44 (1 2016). DOI: 10.3109/21691401.2014.953633.

[47] M. B. et al. "Liposome and lipid bilayer arrays towards biosensong applications." In: *Nano micro small biosensors* 6 (2010), 2481–2497. DOI: 10.1002/smll.201000644.

[48] R. V.L.O. C. Y. Elani. "Vesicle-based artificial cells as chemical microreactors with spatially segregated reaction pathways." In: *Nature Communicationsvolume* 5 (2014). DOI: 10.1038/ncomms6305.

[49] K. Academy. Accessed = 03/16/2019. URL: https://www.khanacademy.org/science/electrical-engineering/ee-circuit-analysis-topic/ee-ac-analysis/v/ee-impedance.

[50] S. Exchange. Accessed = 07/13/2019. URL: https://chemistry.stackexchange.com/questions/59439/correctequation-for-ionic-conductivity-ÃŐz-in-solutions?answertab=active#tab-top.

[51] Y. Xia and G. M. Whitesides. "Soft Lithography." In: *Annual Review of Materials Science* 28 (1998), 153–184. DOI: doi.org/10.1146/annurev.matsci.28.1.153..

[52] G.-P. N. et al. "Biosensors Based on Microfluidic Devices Lab-on-a-Chip and Microfluidic Technology." In: *Nanotechnology and Biosensors* (2018), 375–398. DOI: doi.org/10.1016/B978-0-12-813855-7.00013-1.

[53] H. K.T. C. J. Noh. "Biosensors in Microfluidic Chips." In: *Microfluidics* (2011), 117–1528.

[54] M. Angelova and D. Dimitrov. "Liposome Electro formation." In: *Fraday Discuss. Chem. Soc* 81 (1986). ISSN: 303-311. DOI: 10.1039/DC9868100303.

[55] M. Angeloval. "Preparation of giant vesicles by external AC electric fields. Kinetics and applications." In: *Trends in Colloid and Interface Science VI. Progress in Colloid Polymer Science* 89 (2007). DOI: 10.1007/BFb0116295.

[56] T. Herling. "Integration and characterization of solid wall electrodes in microfluidic devices fabricated in a single photolithography step." In: *Appl. Phys. Lett* 102.184102 (2013). DOI: doi.org/10.1063/1.4803917.

[57] Nupack. Accessed = 07/01/2019. URL: http://www.nupack.org.

[58] N. Yandrapalli and T. Robinson. "Ultra-high capacity microfluidic trapping of giant vesicles for high-throughput membrane studies." In: *Lab Chip* 19.626 (2019). DOI: 10.1039/c8lc01275j.

APPENDIX A

Appendix 1 Differential Scan Calorimetry

DSC analysis was performed on a Perkin Elmer DSC 4000 machine. The measures were done using the following program unless specified otherwise: cooling to -50 °C at a rate of 10 °C/min followed by an isothermal for 2 min; heating from -50 °C to 130 °C at a rate of 10 °C/min followed by an isothermal for 2 min; cooling to -50 °C followed by an isothermal for 2 minutes; heating to 130 °C again at 10 °C/min. The data was extracted from the second heating cycle, the first cycle serving to erase any thermal history present in the material.

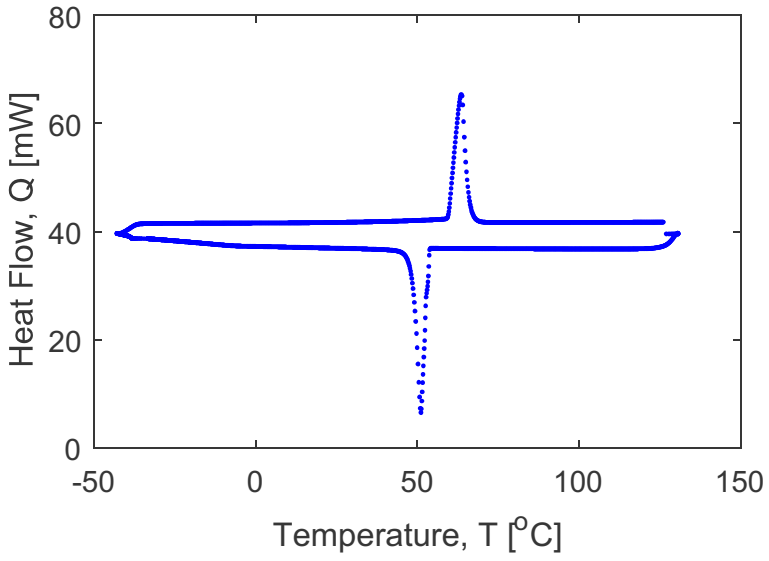

Figure A.1: Alloy DSC analysis: The alloy was submited to a cooling and then heating as explained in the main text. The melting temperature was calculated as the middle point between the two peaks and is 55°C. The lower line corrsponds to cooling step and upper line corresponds to heating step.

APPENDIX B

Appendix 2 Designs speciffication sheets

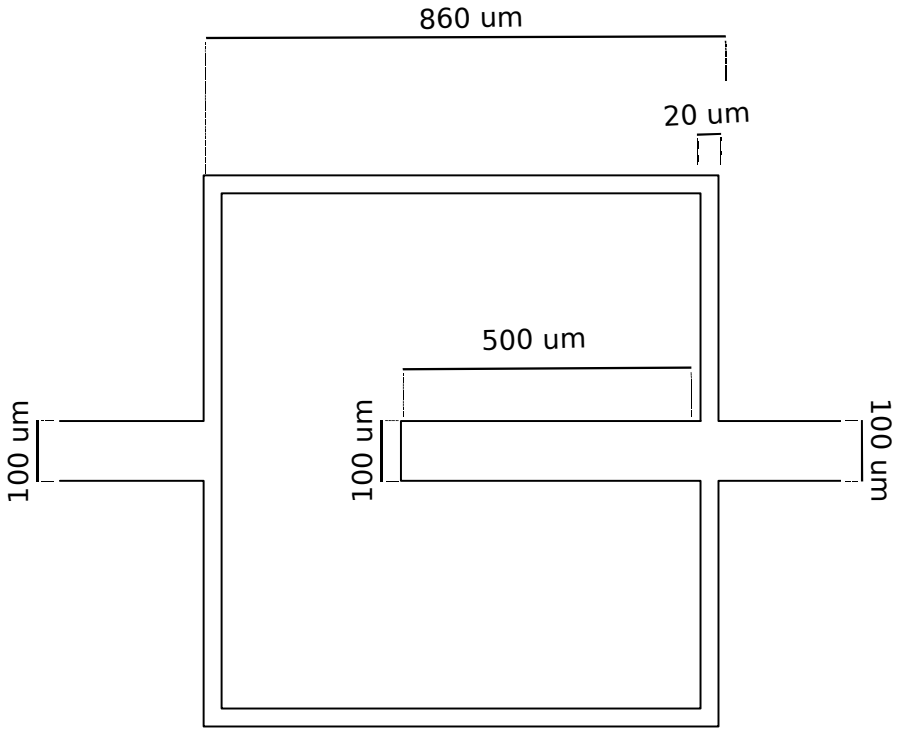

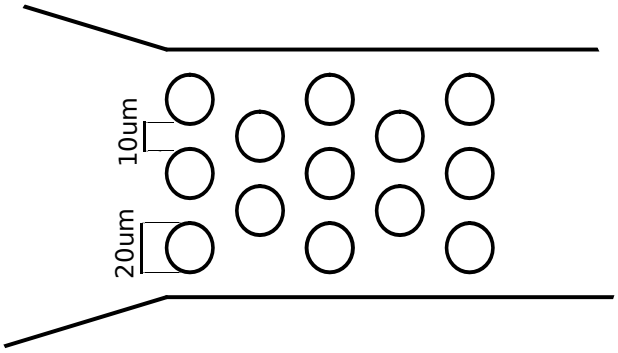
10um
20um

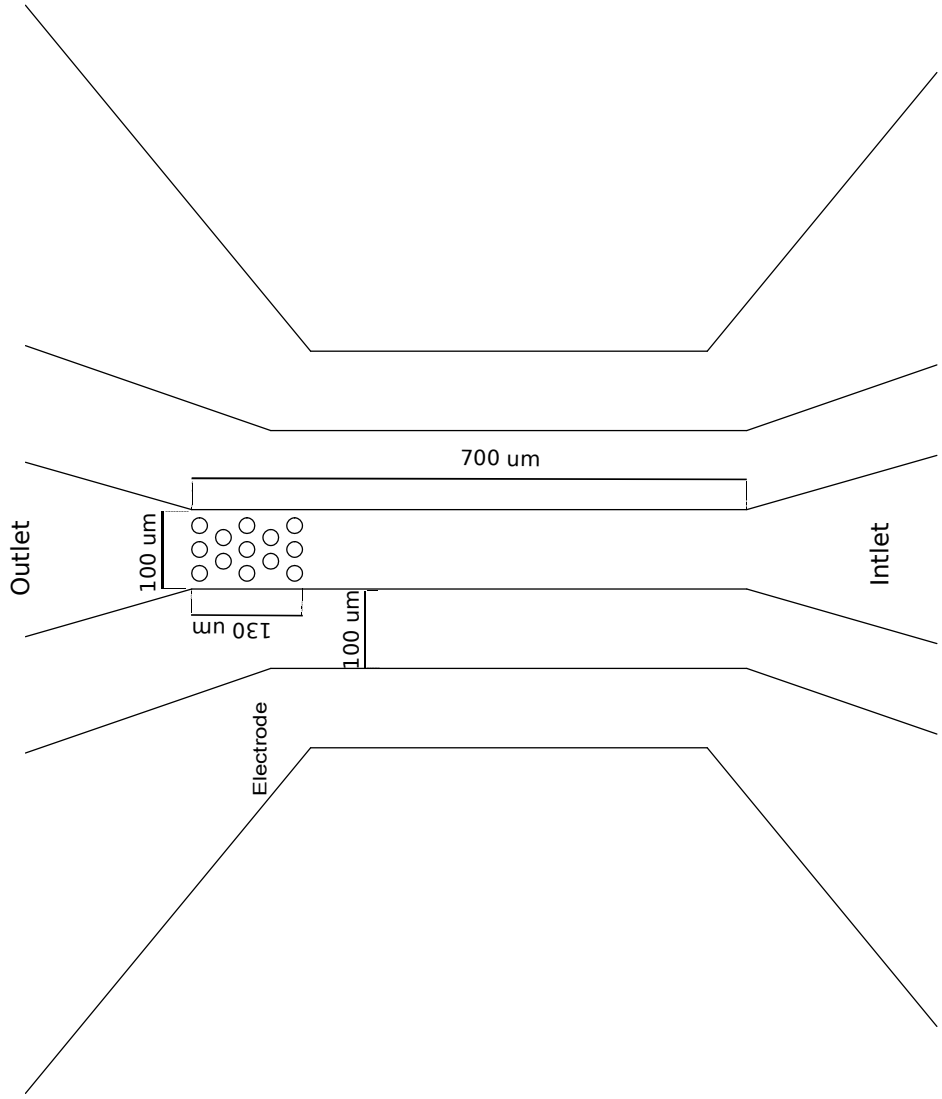
700 um
Outlet
100 um
130 um
100 um
Intlet
Electrode

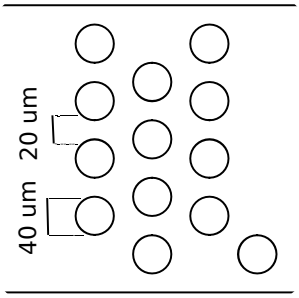
20 um
40 um

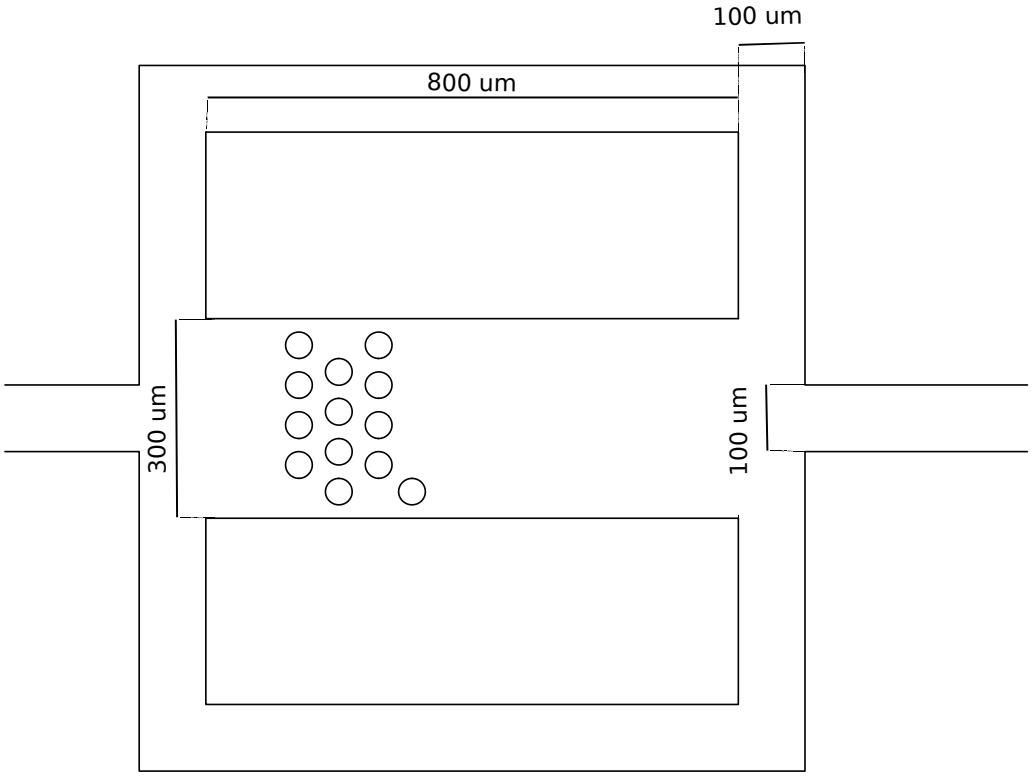
100 um
800 um
300 um
100 um

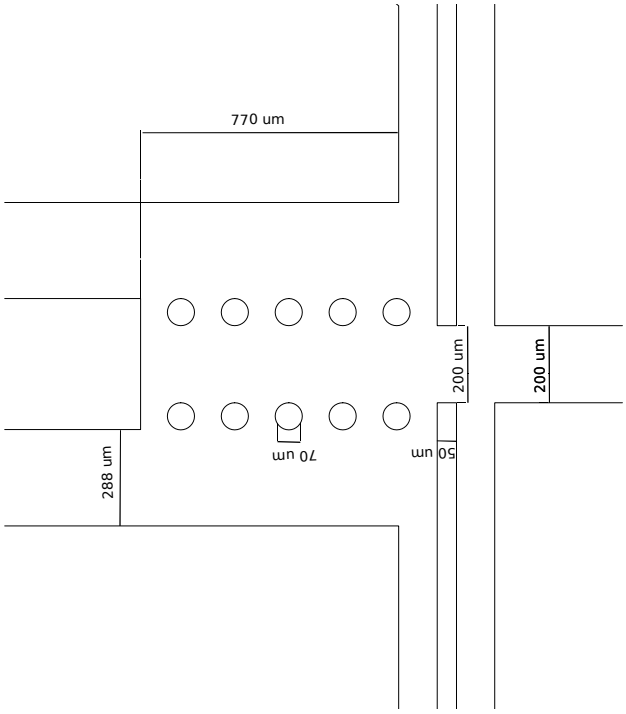
770 um
200 um
200 um
288 um
70 um
50 um

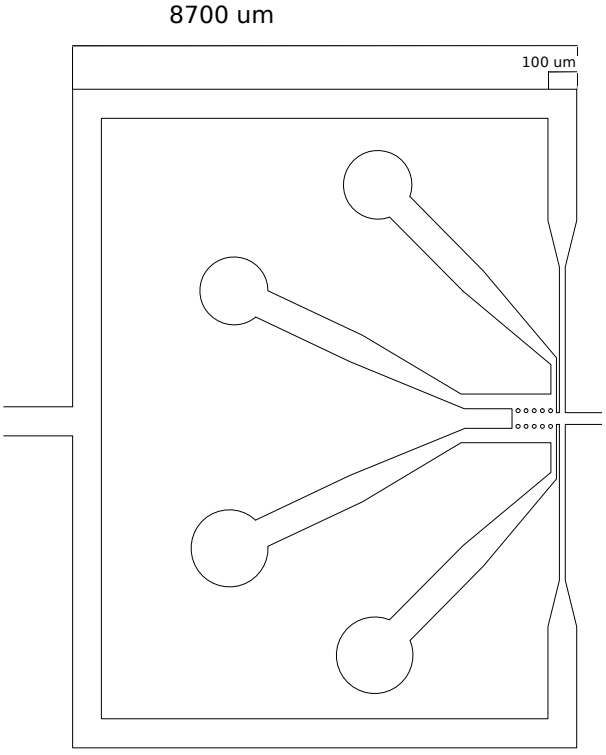
8700 um
100 um

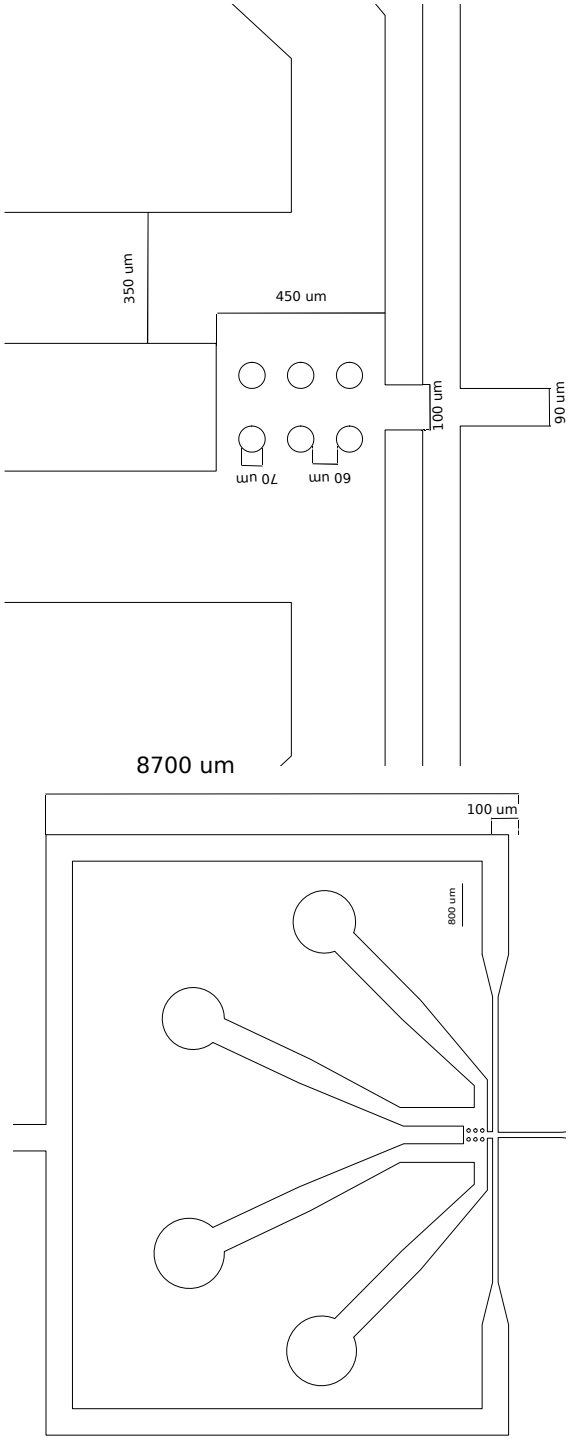
350 um
450 um
100 um
90 um
70 um
60 um
8700 um
100 um
800 um

Appendix 3 DNA system strands

Table C.1: DNA system sequences

Structure	Sequence
B_b	CATCTCACTACTCAACAC CACACTCACCACCACAAC chol
B_{bb}	chol GTTGTGGTGGTGAGTGTG
A	GTGTTGAGTAGTGAGATG TCGGTCGC
C_b	chol CAATCACACCACAAACAC CCAACACAACAACAAACC
C_{bb}	GTGTTTGTGGTGTGATTG chol
B	GCTGTCGC GGTTTGTTGTTGTGTTGG
Linker	GCGACAGC GCGACCGA